

## A review of MEMS oscillators for frequency reference and timing applications

This article has been downloaded from IOPscience. Please scroll down to see the full text article.

2012 J. Micromech. Microeng. 22 013001

(<http://iopscience.iop.org/0960-1317/22/1/013001>)

View [the table of contents for this issue](#), or go to the [journal homepage](#) for more

Download details:

IP Address: 157.89.65.129

The article was downloaded on 08/03/2013 at 15:36

Please note that [terms and conditions apply](#).

## TOPICAL REVIEW

# A review of MEMS oscillators for frequency reference and timing applications

J T M van Beek<sup>1</sup> and R Puers<sup>2</sup><sup>1</sup> NXP Semiconductors, Eindhoven, the Netherlands<sup>2</sup> Department of Electrical Engineering, Katholieke Universiteit Leuven, Heverlee, BelgiumE-mail: [j.t.m.van.beek@nxp.com](mailto:j.t.m.van.beek@nxp.com)

Received 9 April 2011, in final form 16 September 2011

Published 20 December 2011

Online at [stacks.iop.org/JMM/22/013001](http://stacks.iop.org/JMM/22/013001)

## Abstract

MEMS-based oscillators are an emerging class of highly miniaturized, batch manufacturable timing devices that can rival the electrical performance of well-established quartz-based oscillators. In this review, a description is given of the key properties of a MEMS resonator that determine the overall performance of a MEMS oscillator. Piezoelectric, capacitive and active resonator transduction methods are compared and their impact on oscillator noise and power dissipation is explained. An overview is given of the performance of MEMS resonators and MEMS-based oscillators that have been demonstrated to date. Mechanisms that affect the frequency stability of the resonator, such as temperature-induced frequency drift, are explained and an overview is given of methods that have been demonstrated to improve the frequency stability. The aforementioned performance indicators of MEMS-based oscillators are benchmarked against established quartz and CMOS technologies.

(Some figures in this article are in colour only in the electronic version)

## 1. Introduction

Reference oscillators are ubiquitous elements used in almost any electronics system and constitute a multi-billion dollar market in today's electronic industry. These oscillators are used for a wide range of applications varying from keeping track of real time, setting clock frequency for digital data transmission, frequency up- and down conversion in RF transceivers and clocking of logic circuits. Obviously, the electrical specification of the oscillator depends on the application it is being used for. As a result, a variety of oscillator technologies exist today, each technology suiting a specific need. For mainstream consumer-type applications, two technology families are distinguished: mechanical and electrical oscillators. In mechanical oscillators, the frequency-selective element is a mechanical resonator made from quartz for high-end applications (e.g. wireless communication, real-time clocks, high-speed digital interfaces) [1], or other type

of bulk piezoelectric material, such as barium titanate or lead-zirconium titanate, for less demanding and cost-sensitive applications (e.g. digital audio, video, household appliances) [2]. In electrical oscillators, the frequency-selective element is integrated on the chip and comprises an  $R$ - $C$  or a  $g_m$ - $C$  filter for low-end applications (e.g. clocking of logic) or an inductor-capacitor (LC) filter for more demanding applications (e.g. in frequency synthesizers for wireless communication and digital interfaces). In general, the following properties are important for any oscillator technology:

- *Non-deterministic frequency stability*: the frequency spectrum of an oscillator should ideally contain only a single frequency. In reality, the frequency of any oscillator shows short-term frequency fluctuation and hence a broadening of the frequency spectrum. This broadening is expressed in terms of phase-noise or jitter. These short-term fluctuations are caused by non-deterministic noise sources, such as flicker and white noise present

in the oscillator loop. The noise is filtered out in the oscillator loop by the frequency-selective element. An important figure of merit in this respect is the quality factor ( $Q$ -factor) of the frequency-selective element. High  $Q$ -factors translate into a narrow band filtering of the oscillator noise and are therefore beneficial in attaining low jitter or phase-noise. Mechanical resonators exhibit very high  $Q$ -factors up to several million, while LC-based filters show a  $Q$ -factor of about 10 and  $R$ - $C$  or  $g_m$ - $C$  filters show a  $Q$  of less than 1.

- *Power dissipation:* obviously, the oscillator should consume a minimum amount of power. However, a certain amount of power is required to generate sufficient gain in the oscillator loop in order to sustain the oscillation. Furthermore, the signal power should be sufficiently large to have a large signal-to-noise ratio and hence a low jitter and phase noise. The power dissipation for low frequency (i.e. 32 kHz) quartz oscillators for real-time clocks used in watches can be as low as 100 nW, but can be as high as several hundreds of mW for high frequency (i.e. several GHz), low jitter LC-based oscillators and frequency synthesizers.
- *Deterministic frequency stability:* the frequency of the oscillator should be stable under varying environmental conditions such as fluctuations in temperature and supply voltage. Furthermore, the output frequency should be stable over time even in the absence of varying ambient conditions, i.e. the oscillator should exhibit very limited or no aging. The deterministic frequency stability can be as low as a few parts-per-million (ppm) for quartz-based oscillators and is typically more than a few hundred ppm up to a few thousand ppm for CMOS-based oscillators. An important reason for the superior stability of a quartz-based oscillator lies in the fact that certain crystal cuts of quartz exhibit a low temperature drift. The low temperature drift in combination with the high  $Q$ -factor results in a stable oscillation frequency, since the high resonator  $Q$  makes that the oscillation frequency is solely determined by the stability or drift of the resonator.
- *Frequency accuracy:* the frequency of the oscillator should not only be stable but also be accurate, i.e. the oscillator should have a predefined output frequency. The accuracy of this pre-defined frequency is limited by manufacturing tolerances, but frequency trimming can be used to reach the predefined frequency with sufficiently high accuracy. In practice, the frequency accuracy and stability specification are often combined into one single specification.
- *System integration and miniaturization:* almost any electronic system follows the trend of miniaturization and/or higher levels of functionalization. The components that build up these systems should be made smaller and allow for higher levels of system integration in order to accommodate this omnipresent trend. Therefore, the oscillator should be as small as possible, but more importantly should be easy to integrate with other components on the board-, package- or chip level.  $R$ - $C$  or  $g_m$ - $C$  based oscillators can easily be integrated into











CMOS, but typically have a poor performance. LC-based oscillators can also be integrated in CMOS, but require a high quality inductor, which consumes more chip real estate. Although quartz has a superior electrical performance it cannot be integrated onto CMOS and is cumbersome to integrate into the same package as the CMOS chip, since it needs to reside in a cavity in order not to obstruct its mechanical movement during operation.

- *Manufacturing cost:* oscillators are presently being produced in multi-billion quantities annually and typically constitute only a small part of the total bill-of-materials of the electronic system in which they are utilized. Therefore, the commercial success of any new oscillator technology depends highly on whether it can be produced in large volumes at low cost. Quartz or any other mechanical resonator requires a special cavity package. This type of package is a cost adder compared to electrical oscillators that can be integrated on-chip and are packaged using a standard IC package.

Although the electrical performance of mechanical oscillators cannot be met by electrical oscillators, conventional mechanical oscillators show some important drawbacks that prevent their use in any application. Conventional mechanical resonators are relatively bulky and cannot be integrated on a CMOS die and are difficult to integrate into the same package that contains the CMOS die without increasing the manufacturing complexity and cost. Therefore, mechanical resonators have to interface with other circuit components on board level and hence they form a bottleneck for the ultimate miniaturization of the electronic system. In contrast, the use of electrical oscillators is limited to applications where accuracy and noise specification is relaxed. Their stability and phase noise can be improved by locking them to mechanical oscillators using a phase-locked loop (PLL) [3]. However, this again requires a bulky off chip component adding to the total size and cost of the system. In summary, the pros and cons of present day electrical and mechanical oscillators can schematically be depicted as in table 1.

An emerging class of mechanical oscillators is based on MEMS technology [4–6]. The extraordinary small size, high level of integration, low cost and high volume manufacturing capability that is possible with MEMS appear to open exceptional possibilities for creating miniature-scale precision oscillators at low cost. MEMS oscillators can be integrated either on the CMOS die or as a separate die combined with a CMOS die in a single package using a standard low cost plastic package. It can be expected that a MEMS-based oscillator has a superior noise performance and frequency stability compared to electrical oscillators, since the MEMS-based oscillator is based on mechanical resonance exhibiting a high  $Q$ -factor. At the same time, it is expected that the use of MEMS reduces the size and cost and increases the level of system integration compared to the more conventional mechanical resonators, since the processes and materials being used are often CMOS compatible and use the CMOS manufacturing infrastructure. It appears that MEMS fill the gap between high-performance, non-CMOS compatible technologies on the one hand, and low-performance CMOS compatible technologies on the other

**Table 1.** Pros and cons of present day electrical and mechanical oscillators. For explanation of  $FOM_2$ , see section 3.3.

Resonator technology	Accuracy $df/f_0$ (ppm)	Noise $FOM_2$	Size $L \times W \times H$ (mm)	System integration
mechanical	<10 	~130 	>1.6x1.2x0.35 	<ul style="list-style-type: none"> <li>•Bulky hermetic package </li> <li>•Non-CMOS compatible </li> </ul>
electrical	>100 	~90 	<0.5x0.5x0 	<ul style="list-style-type: none"> <li>•Standard plastic package </li> <li>•CMOS design </li> </ul>

hand. The replacement of a quartz resonator with a MEMS resonator and integrating the MEMS resonator with the CMOS in a single package or a single die will lead to a reduction in the form factor, board complexity and bill-of-materials of electronic circuits. Simultaneously, a MEMS implementation will have an improved electrical performance compared to LC, resistor-capacitor (RC) or other types of oscillators based on electrical rather than mechanical resonance. These unique attributes reduce the size and cost of existing electronic systems [7], but might in addition open up new application domains requiring extreme form factor such as their use in wireless sensor nodes [8], SIM and smartcards.

Several review papers related to MEMS-based oscillators have been published in the past. In [4], an extensive overview is given of capacitive resonators; however, their application in oscillators is only briefly discussed and a benchmark with other types of MEMS, CMOS and quartz-based oscillators is not covered. In [5], the focus is on market and business aspects of MEMS oscillators and it does not cover technical aspects of MEMS oscillators. In [6], an overview is given of the key aspects of oscillators based on capacitive transduced MEMS resonators. However, reference [6] does not explain intrinsic physical limitations of capacitive transduced MEMS-based oscillators in comparison to alternative oscillator concepts. In this review, an in-depth, complete and insightful technical overview is given of the state-of-the-art MEMS oscillators. Different resonator transduction schemes are compared and their key properties such as electrical impedance,  $Q$ -factor, thermal drift, power handling and resonator package are explained. On the basis of simple models, these resonator properties are translated into key performance indicators at oscillator level, such as noise performance, power consumption and system level partitioning and integration. These performance aspects are benchmarked and conclusions are drawn on their value, both absolute and relative to well-established oscillator technologies, such as quartz- and CMOS-based oscillators.

## 2. Resonator process integration and packaging

Key benefits of MEMS over quartz-based oscillators are related to the way MEMS resonators are manufactured. A good understanding of the manufacturing process is therefore essential in appreciating the value of MEMS-based oscillators. The wafer level, batch type of fabrication used in MEMS allows for the realization of small and low cost resonators that enable higher levels of system integration. This not only holds

for the resonator itself, but also for the package it is residing in. In this section, the methods and requirements of MEMS resonator manufacturing are discussed and compared to the way quartz resonators are made.

### 2.1. Processing of quartz resonators

A mechanical resonator needs to reside in a cavity in order not to obstruct their mechanical movement during operation. The cavity should be hermetic so as to ensure a stable environment and resonance frequency of the resonator. Commercial quartz resonators are sealed in a metal can or ceramic package. An example of such a package is shown in figure 1. In this case, the package contains both the quartz crystal and the CMOS die that is required to drive the resonator. As can be seen from the interior of the package, the assembly is done at component level using a large variety of techniques. In this case, the CMOS die is wire bonded to a multi-layer ceramic substrate and the quartz crystal is suspended in the cavity and glued at the side to the lead frame. Most of the processes used are serial in nature, i.e. products are assembled sequentially. Furthermore, these technologies do not lend themselves well to miniaturization, since they involve the individual handling of very small components.

In contrast, MEMS resonators are batch fabricated on a silicon wafer, i.e. many individual products are manufactured in parallel on a single substrate. A key aspect in the batch fabrication of the MEMS resonator is that formation of the resonator cavity forms an integral part of the wafer-level processing. This is the key differentiating advantage over established quartz technology, since it eliminates the need for the time consuming and costly sequential placement of each individual resonator into the bulky metal can or ceramic package. Furthermore, the on-wafer packaged MEMS resonator is processed on a silicon wafer. In principle, the silicon wafer might contain the CMOS circuitry that is required to drive the resonator or other circuitry that uses the frequency output of the oscillator. Even if the resonator die does not contain the CMOS driver, MEMS technology still benefits from the fact that the die can be separated from the wafer using well-established manufacturing flows used in CMOS industry. The MEMS die can be wire-bonded together with the CMOS die on a standard lead frame and overmolded in plastic using mainstream and low cost molding techniques commonly used for the packaging of CMOS dies.

Although the miniaturization of the resonator will help reduce the overall size of electronic systems and can be

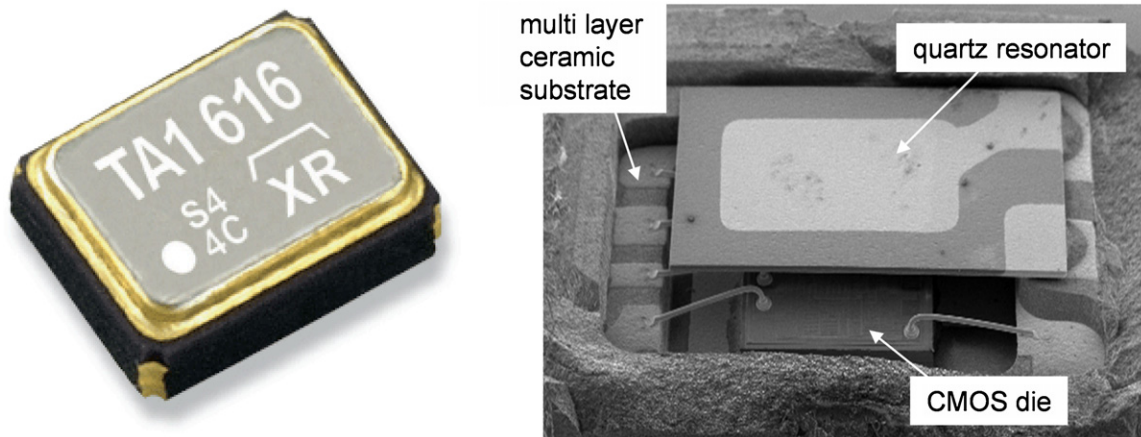


**Figure 1.** Exterior (left) and interior (right) of the Epson Toyocom SG-310 series quartz-based oscillator. The package contains both the quartz crystal and the CMOS die that is required to drive the resonator. The assembly is done at component level using a variety of techniques. The CMOS die is wire bonded to a multi-layer ceramic substrate and the quartz crystal is suspended in the cavity and glued at the side to the lead frame.

beneficial for cost reduction, it sets important limits on the gas pressure inside the resonator cavity. For a fixed resonance frequency, the  $Q$ -factor of the resonator scales with the ratio of the resonator mass and the damping factor. Mass scales with resonator volume and air damping approximately scales with resonator area. Therefore, it can be understood that when the resonator is reduced in size, the effect of air damping on the resonator  $Q$  becomes more prominent, as will be explained in more detail in section 4.2. In practice, the  $Q$ -factor of most MEMS resonators resonating at frequencies below 1 GHz is limited by air damping at atmospheric pressure. Therefore, the cavity pressure should be below atmospheric pressure in order to maximize the  $Q$ -factor in most cases and obviously sets specific requirements on the packaging process. Apart from the benefit of high  $Q$ , it has also been shown that the frequency stability of the resonator can be deteriorated when the resonator is not sealed off hermetically from its environment, as will be explained in more detail in section 5.1. This effect can be attributed to adsorption of foreign material on the resonator surface which causes a detuning of its resonance frequency. This detuning becomes more pronounced when the resonator is scaled down in size and mass, as is the case in MEMS.

## 2.2. MEMS packaging concepts

Two MEMS process families can be distinguished for the batch fabrication of the resonator cavity. The most mature method is based on the bonding of two wafers [10, 11], as is schematically depicted in figure 2. In this case, the wafer containing the MEMS resonator contains a seal ring which is bonded to a seal ring that is present on a capping wafer. A cavity is created around the resonator after bonding the two wafers together. The different resonators are then singulated from the wafer. The bonding process should not contaminate the cavity and should result in a hermetic seal in order to ensure a stable, high  $Q$  resonance frequency of the resonator. Bonding techniques that have been reported that fulfill these requirements are based on anodic bonding [12] and diffusion bonding [11, 13]. These two bonding technologies need a flat

and smooth surface in order to allow for an intimate contact between the two bonding surfaces imperative for ensuring a strong bond. If a flat and smooth surface is not easily obtained as a result of wafer topography from the device process, intermediate malleable materials are required for connecting the cap wafer and the MEMS wafer together. Examples of this type of bond are based on thermo compression bonding of Au-Au [11] and eutectic bonding of Au-Si, Au-Sn, and Al-Si(O<sub>2</sub>) [13–15]. Getter films might be used to getter any residual gasses inside the cavity and maintain the reduced pressure over prolonged periods of time. In [16] it is demonstrated that a vacuum level <100 mTorr can be maintained for 10 years thereby ensuring a sufficiently high resonator  $Q$ -factor over lifetime. It is furthermore demonstrated that the frequency aging can be within 5 ppm over a period of 1 year and after high temperature storage and temperature cycle tests.

Although wafer-to-wafer bonding is a relatively mature technique that is also used for the packaging of e.g. accelerometers and gyroscopes, it has the disadvantage that a large amount of wafer real estate is required for the sealing ring. Sealing ring widths are typically in the range of 100  $\mu\text{m}$  in order to guarantee sufficient hermeticity of the package. This dimension should be compared with the diameter of a typical MEMS resonator which is also in the 100  $\mu\text{m}$  range. Therefore, the area that is occupied by the sealing ring is often many times the area taken up by the MEMS resonator itself. The relatively large sealing ring not only results into a larger product, but also increases the manufacturing cost since fewer resonators can be processed on a single wafer. Furthermore, the height of the packaged resonator is set by the combined thickness of two wafers. Therefore, wafer bonding sealing can lead to a package size that is many times the size of the resonator residing inside the cavity. A more advanced on-wafer sealing method leading to a much smaller package is based on surface micro-machining. A schematic process flow for the fabrication of the resonator cavity using this technique is depicted in figure 3. In this case, the cavity is created through thin film layer deposition and sacrificial layer etching techniques. The advantage of thin film capping is that the



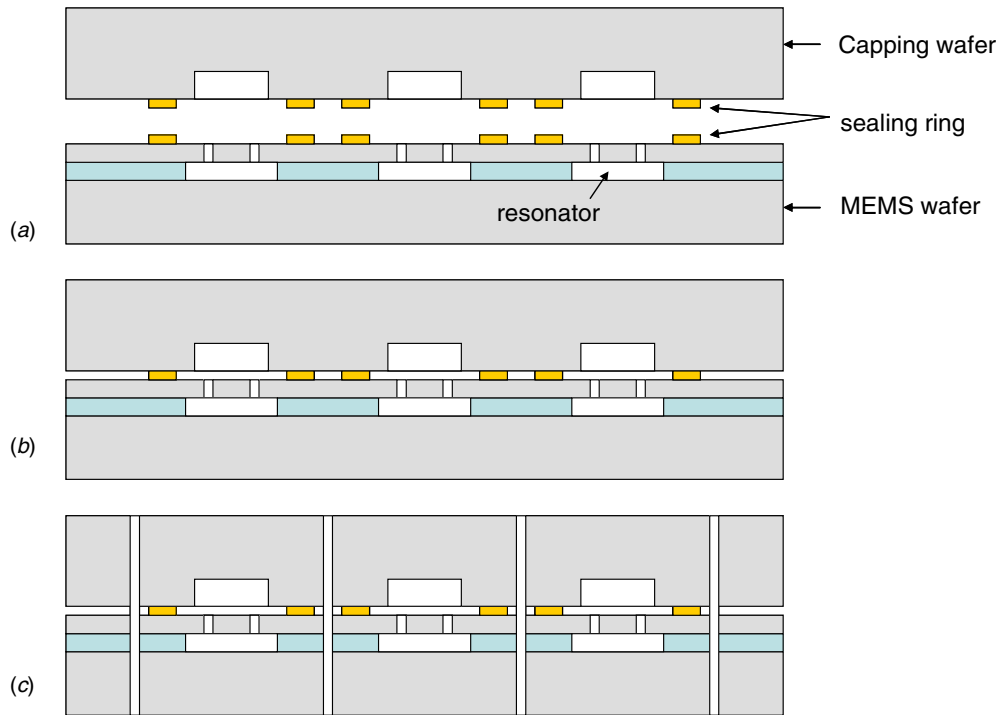


**Figure 2.** Schematic flow of a batch-fabricated resonator that is sealed by means of wafer-to-wafer bonding. The wafer containing the fully released MEMS resonator contains a seal ring which is bonded to a seal ring that is present on a capping wafer (a). A cavity is created around the resonator after bonding the two wafers together (b). The resonator dies are separated from the wafer after bonding (c).

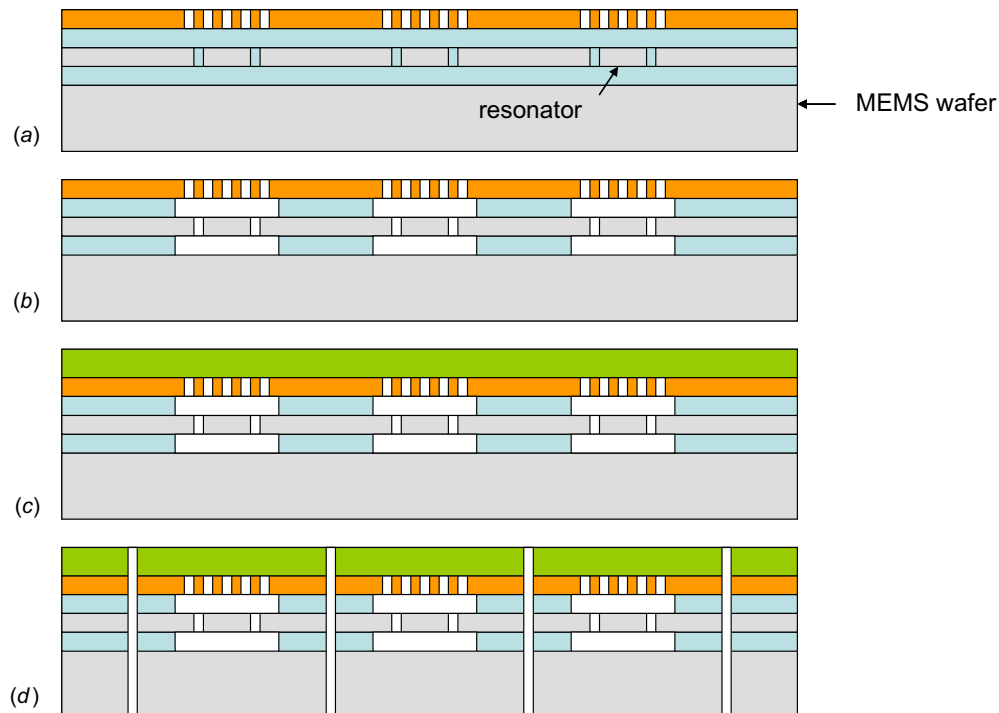


**Figure 3.** Schematic flow of a batch-fabricated resonator that is sealed by means of thin film capping. A layer stack of sacrificial and structural layers is deposited on the wafer (a). The sacrificial layers are etched through the openings in the cap layer (in orange) to release the resonator and the cap layer (b). The openings in the cap layer are sealed by depositing a plug layer (in green) (c). The resonator dies are separated from the wafer using standard wafer dicing techniques (d).

size of the cavity is only slightly larger than the size of the resonator itself. As a result, the die size remains small which will lead to a cost benefit, since a large amount of devices

can be processed onto a single wafer. In figure 4, a focused ion beam (FIB) cross-section of such a thin film cavity is depicted. In this case, the cavity package spans approximately

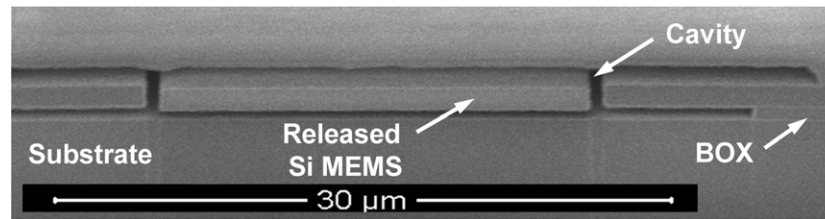


**Figure 4.** FIB cross section SEM image of a cavity and Si MEMS resonator. The resonator is defined on a SOI wafer. The buried oxide (BOX) layer and the sacrificial layer (not shown) on top of the released MEMS have been etched to form the cavity.

50  $\mu\text{m}$ , which is much smaller than what can be obtained with wafer-to-wafer bonding techniques. The height of the sealed resonator is low since it is set by the thickness of a single wafer instead of the combined thickness of two wafers in the case of wafer-to-wafer bonding. The wafer containing the sealed resonators has the same outer dimensions and bond pad layout as any ordinary CMOS wafer and can therefore be handled in standardized CMOS assembly lines for grinding, dicing and plastic over molding of the MEMS die. As a result, the MEMS die can be thinned down to a height in the order of 0.1 mm or less using standard silicon grinding processes without any special effort. This is several times thinner than what can presently be achieved with ceramic or metal can packages used for quartz resonator and can be a key differentiating property when these resonators are integrated in thin objects.

First reports [17, 18] on this type of thin-film packages were based on a poly-silicon cap that is released from the substrate through etching of a silicon dioxide sacrificial layer. In this case, the cavity was sealed by a second poly-silicon layer. The use of poly-Si sacrificial layers with a poly-Si cap has been reported in [19]. In this case, the sacrificial layer and the cap layer are separated by a thin layer of  $\text{SiO}_2$  in order to prevent etching of the cap layer during sacrificial layer etching. A porous Si capping layer can be used to accommodate easy access to the sacrificial layer, which can then be subsequently sealed with a non-porous film to hermetically seal the cavity [20, 21]. Other porous capping layers requiring lower processing temperatures are based on anodized Al [22, 23] and PECVD  $\text{SiOC}$  [24]. Other attempts to lower processing temperature are based on the use of non-permeable PECVD nitride and PECVD oxide capping layers [25–29]. Instead of using  $\text{SiO}_2$  as the sacrificial layer, several other materials have been proposed as well, such as PECVD-deposited carbon fluorides [25]. Thermal degradable polymers are used as the sacrificial layer in [30–32] and allow for the release of the capping layer simply by heating the wafer. The use of an electroplated capping layer is reported in [33].

The above-mentioned references are suitable for capping MEMS resonators made from Si. As will be explained later, it can be beneficial to include a piezoelectric layer in the resonator, such as AlN, in order to lower its impedance. Obviously, this places restrictions on the materials and etch processes being used for processing the thin-film cavity. In [34, 35] process flows are described that are compatible with the AlN-based resonator, the process flow in [34] uses the SU-8 epoxy capping layer while in [35] a flow is described

for processing an AlN-based resonator using a PECVD nitride capping layer.

Although this type of thin film packaging is very promising for MEMS resonators and several process flows have been described for the processing of these micro-cavities, very limited data are available on the reliability and lifetime of such micro-cavities. One exception is a flow described in [36–39], called the ‘epi-seal’ method that uses a 20–50  $\mu\text{m}$  thick poly-Si capping layer grown in an epi-reactor at a relatively high temperature of 980  $^\circ\text{C}$ . Using the epi-seal method, the cavity pressure during long-term monitoring performed at room temperature shows no measurable pressure change, while at 100  $^\circ\text{C}$  in a normal atmosphere the encapsulated cavity pressure increased at a rate of only 5–10 mTorr/year. Furthermore, it is shown that the frequency aging of the resonator is within 1 ppm per year [40, 41], which is less than what is typically observed for quartz resonators.

### 2.3. Co-integration of MEMS with CMOS

To make up an oscillator, the packaged resonator should be combined with a driver circuit that is typically realized in CMOS. Obviously, the highest level of integration that can be achieved is to integrate the resonator on the same die that also holds the CMOS circuitry. Several process flows have been described where the MEMS resonators are embedded in an existing CMOS flow [42–44]. However, it remains difficult if not impossible not to compromise the performance of either the CMOS or the MEMS resonator when embedding the process steps for the MEMS between or before the process steps required for processing the CMOS. The most convenient way to achieve monolithic integration of MEMS and CMOS is to stack the dedicated MEMS layers and processing on top of an existing CMOS flow. In this way, the impact on the CMOS is minimized and no dedicated CMOS process development is required for the integration of the MEMS resonator. However, processing temperatures should stay below 450  $^\circ\text{C}$  in order not to interfere with the CMOS circuitry underneath. This temperature limitation prohibits the use of poly- or mono-crystalline silicon for making up the resonator or the thin-film capping. A material shown to have similar mechanical properties as poly-Si while allowing processing at sufficiently low temperatures is LPCVD or PECVD SiGe. In [45], a 14 kHz poly SiGe resonator is processed on top of a CMOS wafer yielding functional oscillators. The use of SiGe as the capping layer for packaging of MEMS is discussed and demonstrated in [46, 47]. Cavity pressures of 1 Pa have

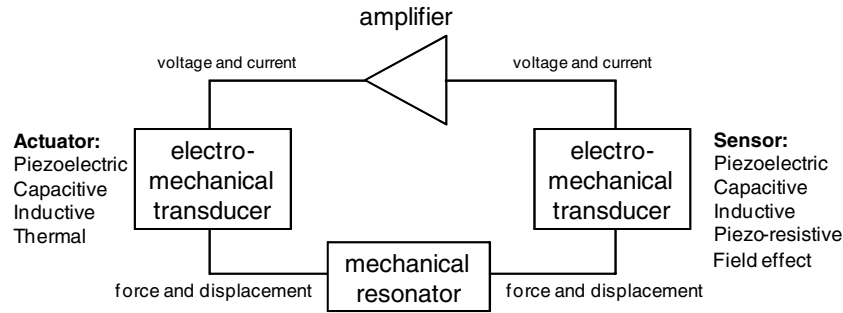


**Figure 5.** Basic principle of an electro-mechanical oscillator. Different forms of electro-mechanical transduction can be used.

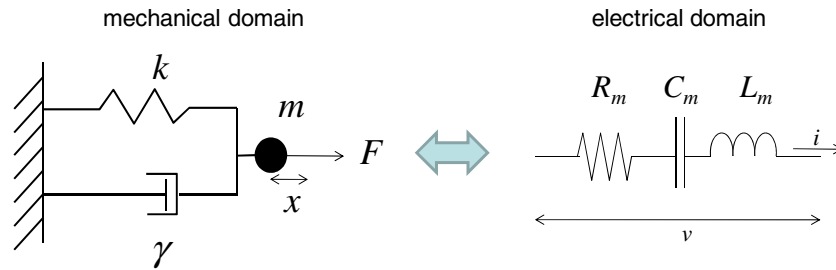


**Figure 6.** A piezoelectric or capacitive MEMS resonator can be modeled in the mechanical domain by a mass  $m$ , stiffness  $k$ , and damping factor  $\gamma$ . In the electric domain, the same resonator can be modeled by an equivalent resistance  $R_m$ , inductance  $L_m$ , and capacitance  $C_m$  connected in series.

been maintained over a period of at least several months by sealing the SiGe cap with PVD Al [47]. Ni is another material that can be deposited at low temperatures using electroplating techniques and has been used for the processing of resonators [48]. Piezoelectric resonators comprising sputtered AlN thin films can be processed below 450 °C and therefore allow for the processing on top of CMOS. In [49], an AlN-based GHz FBAR resonator is processed on top of a BiCMOS wafer.

Although attractive from a miniaturization point of view, the monolithic integration of the MEMS resonator can pose an important cost drawback compared to a standalone MEMS die that is combined with a standalone CMOS die in a single IC package. When a relatively small component, such as a MEMS resonator, is added to a rather large CMOS chip the added functionality comes at a relatively high cost, since the number of MEMS devices on a single wafer will be relatively low in comparison to the case where the resonators can be spaced closer together in the absence of the CMOS. The same drawback is valid when a relatively large MEMS component is added to a small IC. It is therefore important that the chip area taken up by the CMOS circuitry matches the chip footprint that is occupied by the MEMS. However, the additional area taken up by bond pads and added assembly costs should be considered as well when the MEMS die is separate from the CMOS die.

### 3. Oscillation condition and non-deterministic frequency stability: general theory

An oscillator consists of a frequency selective element, which is the mechanical resonator, and a gaining element,

which is the feedback amplifier. The feedback or sustaining amplifier is required to sustain a resonance in the frequency selective element. The interface between the resonator and the sustaining amplifier accommodates the transfer of electrical energy into mechanical energy and vice versa. Various ways of transduction are possible, as is depicted in figure 5 and described in [50]. MEMS oscillators have been demonstrated using a variety of transduction principles, but the most commonly used transduction is piezoelectric or capacitive. This section explains how the oscillator performance is determined by certain resonator parameters, namely resonator impedance level, power handling and  $Q$ -factor in case piezoelectric or capacitive transduction is used.

#### 3.1. Resonator impedance and $Q$ -factor

The resonators based on piezoelectric or capacitive transduction can be modeled in the electric domain by an equivalent resistance  $R_m$ , an inductance  $L_m$  and a capacitance  $C_m$  connected in series [9, 51, 52]. The electronic equivalent elements capture respectively the damping coefficient  $\gamma$ , the mass  $m$  and stiffness  $k$  of the resonator, as is schematically depicted in figure 6. This relationship can be understood by considering the equation of motion of a mass-spring system that is excited by an alternating force,  $F$ :

$$m\ddot{x} + \gamma\dot{x} + kx = F. \quad (1)$$

The displacement  $x$  and the force can be expressed in an ac current  $i$  going through the resonator and ac voltage drop  $v$  over the two resonator terminals by means of the electro-mechanical coupling factor. The coupling factor is an important parameter



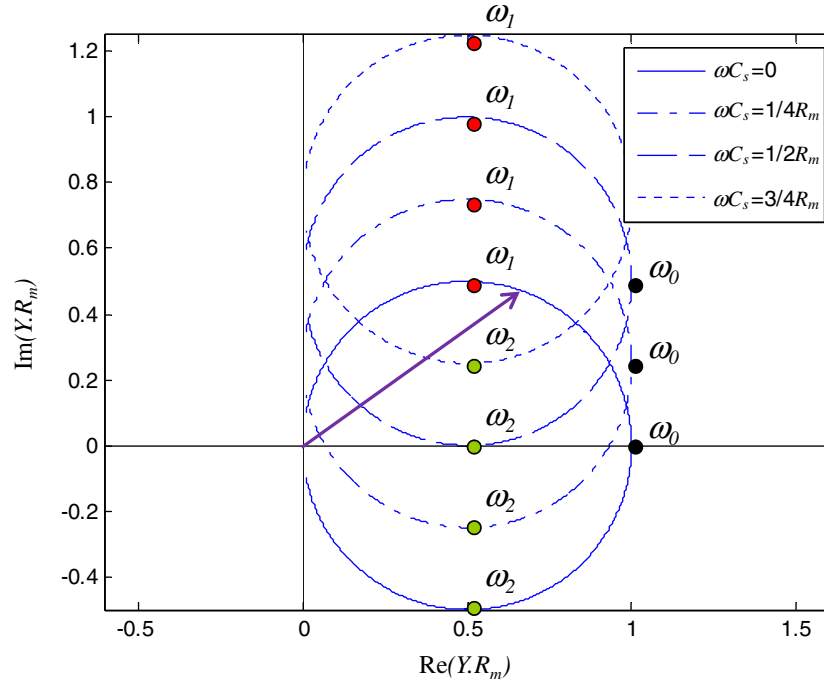


**Figure 7.** Polar plot of resonator admittance  $Y_m$  normalized to  $1/R_m$  for different values of the shunt capacitor  $C_s$ .

determining the overall oscillator performance and depends on resonance mode, electrode configuration and material properties, in the case of piezoelectric materials and bias voltage in the case of electrostatic transduction, as will be explained in section 4.1. The coupling factor is defined as the ratio of displaced charge and spatial displacement,  $\eta = q/x$ , and can be expressed alternatively as

$$\dot{x} = \frac{i}{\eta}. \quad (2)$$

Appreciating the fact that the power that is dissipated in the resonator can be written as the product  $v \cdot i$  in the electrical domain and as  $F\dot{x}$  in the mechanical domain results in

$$F = \eta v. \quad (3)$$

Now, the equation of motion can be expressed in terms of alternating current and voltage by combining (1)–(3):

$$L_m \frac{\partial i}{\partial t} + R_m i + \frac{1}{C_m} \int i dt = v, \quad (4)$$

in which the mechanical equivalent inductance  $L_m$ , capacitance  $C_m$  and resistance  $R_m$  are expressed as

$$L_m = \frac{m}{\eta^2} \quad (5)$$

$$C_m = \frac{\eta^2}{k} \quad (6)$$

$$R_m = \frac{\gamma}{\eta^2}. \quad (7)$$

From (4) it can be concluded that the resonator can be represented by a series branch of an inductor  $L_m$ , capacitor  $C_m$

and resistor  $R_m$ . The resonance frequency  $\omega_0$  of this system is given by

$$\omega_0 = \sqrt{\frac{k}{m}} = \frac{1}{\sqrt{L_m C_m}}. \quad (8)$$

In most cases also a shunt capacitance  $C_s$  is present between the two resonator terminals in parallel to the series  $L_m$ – $R_m$ – $C_m$  branch. The shunt capacitance is caused either by the dielectric permittivity of the resonator itself or by on-chip and off-chip parasitic impedance. The admittance of the resonator including the shunt capacitor is therefore given by

$$Y = j\omega C_s + \frac{1}{j\omega L_m + 1/j\omega C_m + R_m}. \quad (9)$$

The phase and magnitude behavior of the admittance can conveniently be analyzed by plotting admittance in the complex plane, as is shown in figure 7. A circle results when plotting the real part of the admittance versus the imaginary part of the  $R_m$ – $C_m$ – $L_m$  branch for frequencies close to the resonance frequency,  $\omega_0$ . The circle is translated along the imaginary axis by an amount equal to the shunt admittance  $j\omega C_s$  when plotting the total admittance, as is evident from (9). In figure 7, the total admittance normalized to  $R_m$  is plotted when the shunt impedance is 0, 0.25, 0.5 and 0.75 times the value of  $R_m$ . Each point on the circle corresponds to a frequency  $\omega$  and the circle is followed in the clockwise direction when  $\omega$  is increased. Plots of the phase and magnitude versus frequency can easily be constructed from figure 7. For a certain  $\omega$ , a vector can be drawn from the origin to a point  $Y(\omega)$  on the admittance circle. The phase of the admittance is defined by the angle of the vector with the real axis and the magnitude of the admittance is represented by the length of the vector. Magnitude and phase as a function of  $\omega$  as derived from figure 7 are plotted in figure 8. These plots

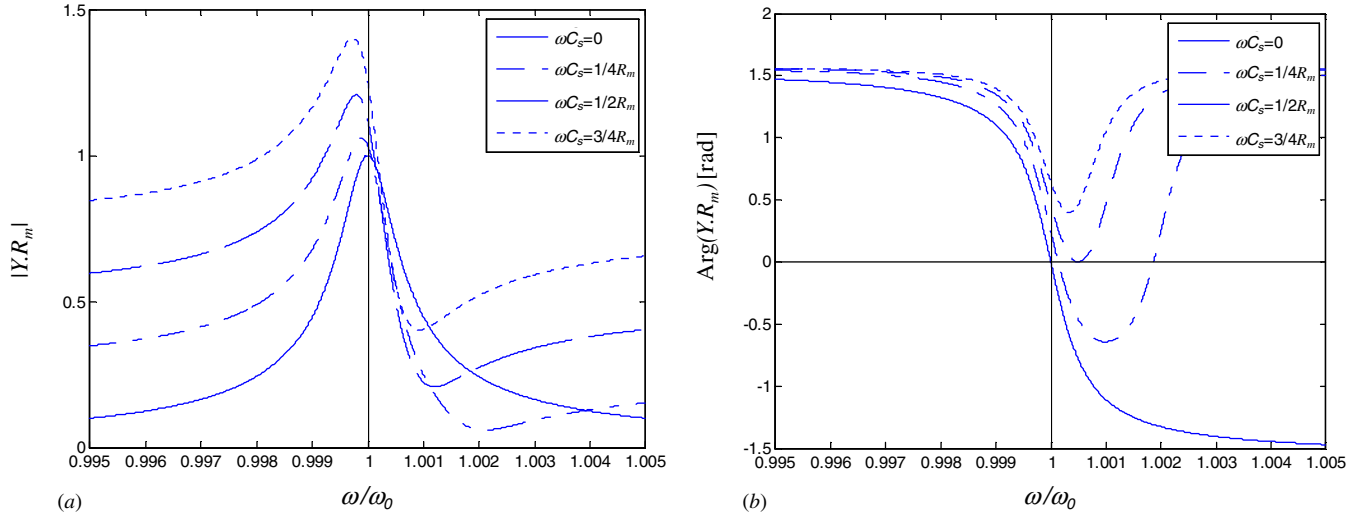


**Figure 8.** (a) Magnitude and (b) phase of resonator admittance as a function of frequency as derived from the polar plot shown in figure 7. The admittance is normalized to  $1/R_m$ .

give insight in the condition for starting the oscillation as well as the noise behavior of the oscillator as will be explained in sections 3.2 and 3.3.

The resonator  $Q$ -factor is an important parameter determining the phase noise performance of the oscillator, as will be explained in section 3.3, but is often defined in different ways. The unloaded  $Q$  or mechanical  $Q$  of the resonator,  $Q_{\text{unloaded}}$ , is defined as the ratio of energy stored,  $E_{\text{stored}}$  in the resonator divided by the energy dissipated caused by mechanical damping during one period of resonance,  $E_{\text{diss}}$ . In terms of mechanical and electrical properties of the resonator, this translates into

$$Q_{\text{unloaded}} = 2\pi \frac{E_{\text{stored}}}{E_{\text{diss}}} = \frac{\sqrt{km}}{\gamma} = \frac{1}{R_m} \sqrt{\frac{L_m}{C_m}}. \quad (10)$$

The unloaded  $Q$ -factor is not dependent on the coupling factor, since it is set solely by the mechanical parameters of the resonator itself. The unloaded  $Q$ -factor can also be derived graphically from figure 7 and is equal to  $Q_{\text{unloaded}} = \omega_0/(\omega_2 - \omega_1)$ , i.e. the frequency  $\omega_0$  where the motional admittance has its maximum divided by the frequency difference  $\omega_2 - \omega_1$  where the motional admittance at  $\omega_1$  and  $\omega_2$  is  $1/\sqrt{2}$  times the admittance at  $\omega_0$ .

### 3.2. Oscillation condition and oscillation frequency

An oscillator needs to fulfill four oscillation criteria in order to sustain a stable oscillation. Two criteria need to be fulfilled to enable oscillation and two additional criteria are required to ensure stability of the oscillation [51]. The oscillation criteria that enable any oscillation state that the open loop gain  $G$  at the oscillation frequency  $\omega_s$  and oscillation amplitude  $a_s$  equals unity. Furthermore, the phase shift in the oscillator loop should be equal to a multiple of  $360^\circ$ . When the loop gain is expressed in the complex plane, the oscillation criteria simply state that the real part of the loop gain  $G$  equals unity and the imaginary part equals zero:

$$\text{Re}(G(\omega_s, a_s)) = 1 \quad (11)$$

$$\text{Im}(G(\omega_s, a_s)) = 0. \quad (12)$$

When an oscillator meets the criteria described by (11), (12), the oscillation will start but does not necessarily result in a stable oscillation. The following two additional criteria need to be met to ensure a stable oscillation:

$$\left. \frac{\partial (\arg G)}{\partial \omega} \right|_{\omega_s, a_s} < 0 \quad (13)$$

$$\left. \frac{\partial |G|}{\partial a} \right|_{\omega_s, a_s} < 0. \quad (14)$$

The first stability condition is that for phase stability and states that when the loop phase increases, the frequency should decrease. No periodic solution can be maintained if this condition is not fulfilled. The second condition is that of amplitude stability. This condition ensures that the amplitude of the oscillation is self-limiting which is the case when the loop gain decreases when the amplitude increases.

The loop gain is defined by the combined transfer of the resonator and the sustaining amplifier. It therefore depends on the amplifier topology being applied [51, 53]. The amplifier topology that is most easy to analyze is the transimpedance amplifier (TIA) with buffered output, as is shown in figure 9(a). A convenient property of this amplifier topology is that both its input and output impedances equal zero. The zero output impedance makes the amplifier output an ideal voltage source, while the zero input impedance makes that the voltage drop over the two resonator terminals is equal to the voltage generated at the amplifier output. Therefore, the small signal equivalent of the TIA can be represented by a current-controlled voltage source (CCVS), as is depicted in figure 9(b). In the following, the conditions for oscillation and the noise behavior of this particular oscillator topology are analyzed based on the resonator model derived in section 3.1. Although other configurations of the amplifier are possible and used in practice, the expressions derived for this particular oscillator are similar to expressions derived for other oscillator topologies [51, 54, 55].

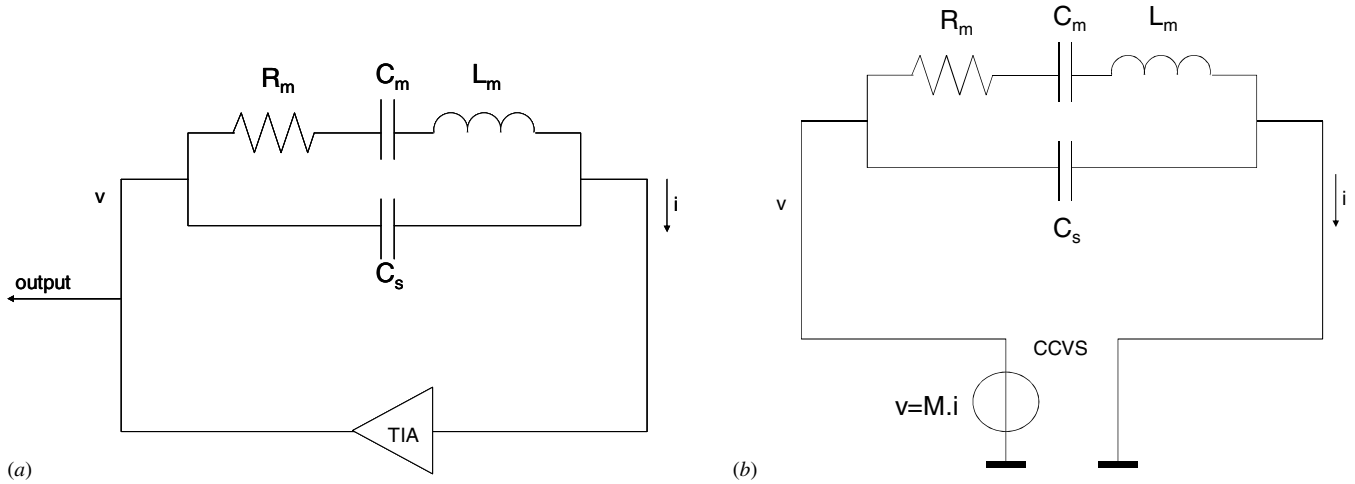


**Figure 9.** (a) Circuit diagram of an oscillator based on a TIA. (b) Small signal model of an oscillator based on a transimpedance amplifier. The amplifier is represented by a CCVS.

The loop gain for the transimpedance oscillator depicted in figure 9 is simply a scalar multiplication of the resonator admittance as described by (9) and is written as  $G = M \cdot Y$  where  $M$  is the amplifier gain expressed in Ohm. Therefore, the oscillation criteria in (11), (12) can be reformulated as

$$\text{Re } Y = \frac{1}{M} \quad (15)$$

$$\text{Im } Y = 0. \quad (16)$$

Two important conclusions can be drawn from these equations. First of all, the admittance of the resonator needs to be real at the oscillation frequency and therefore the locus of the admittance needs to cross the  $x$ -axis in figure 7. Since the diameter of the locus equals  $1/R_m$  and the locus is centered at a distance  $\omega_0 C_s$  above the  $x$ -axis, the following relation should hold:

$$R_m \leq \frac{1}{2\omega_0 C_s}. \quad (17)$$

In other words, the oscillation will not occur when

- motional impedance  $R_m$  is too large,
- resonance frequency  $\omega_0$  is too high and
- shunt capacitance  $C_s$  is too large.

In these situations, the phase condition (12) cannot be met and therefore no condition exists for sustained oscillation. Furthermore, it can be seen from figure 7 that the real part of  $Y$  equals  $1/R_m$ . Therefore, low values of  $R_m$  allow for low values of the amplifier gain  $A$ . Low gain amplifiers typically consume less power; hence, a low motional impedance is helpful in reducing overall power consumption. The relationships mentioned in (15) and (16) set not only the conditions for starting the oscillation, but also the oscillation frequency  $\omega_s$ , since  $Y$  is a function of  $\omega$ . In figure 7, both crossings of the admittance locus with the  $x$ -axis meet the  $\text{Im } Y = 0$  condition, but only the crossing at the right meets the criterion for phase stability described by (13), as is evident from figure 8. From figure 7, it can be seen that the  $\text{Im } Y = 0$  crossing of the admittance locus is identical to the mechanical resonance

frequency when  $C_s = 0$ , but is shifted to the lower part of the circle when  $C_s$  is increased. The frequency difference between the two crossings is given by

$$\frac{\omega_s - \omega_0}{\omega_0} < \frac{1}{2Q_{\text{unloaded}}}. \quad (18)$$

From this relation, it is clear that  $Q$  should be as large as possible in order to have a well-defined oscillation frequency  $\omega_s$  that is very close the mechanical resonance frequency  $\omega_0$  of the resonator. However, some frequency detuning is sometimes preferred, e.g. when compensating for temperature drift of the resonator, see also section 5.1.

### 3.3. Phase noise

Oscillator phase noise can be regarded as the non-deterministic frequency instability of the oscillator's output frequency, since it originates from flicker noise, white noise and other non-deterministic noise sources that are present in the oscillator loop. Noise of the oscillator's wave front can be decomposed in amplitude noise and phase noise. Amplitude noise can typically be filtered out in the oscillator loop and is not a critical parameter for most applications. In contrast, phase noise cannot be filtered out and is an important performance indicator of any oscillator. For digital systems, the oscillator noise is typically specified in terms of jitter. Jitter can be derived from phase noise spectra by integrating an application-specific frequency band of the phase noise spectrum [3].

The effect of the oscillator's components on its phase noise, based on a linear time-invariant model, was first described by Leeson [56]. The derivation of Leeson's model as described in [57] is used here to express the phase noise in terms of resonator properties using the linear feedback system shown in figure 10.  $N$  represents a noise source,  $S$  the oscillation signal and  $G$  is the transfer function of the oscillator loop. If, at frequency  $\omega_s$ , the phase shift across the oscillator loop precisely matches zero or a multiple of  $360^\circ$  and the loop gain matches unity, the closed-loop transfer function

$$\frac{S}{N}(j\omega) = \frac{G(j\omega)}{1 - G(j\omega)} \quad (19)$$

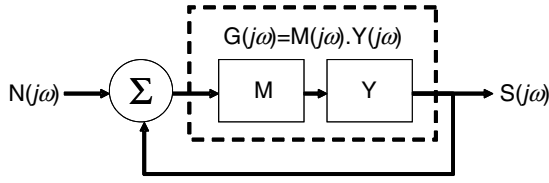


**Figure 10.** Oscillator represented by a linear feedback system. Noise  $N(s)$  is inserted in the feedback loop and transferred to oscillator noise by the transfer function of the amplifier  $M(s)$  and resonator  $Y(s)$ . Loop gain  $G(s)$  is defined as the combined transfer of  $M(s)$  and  $Y(s)$ .

goes to infinity and an oscillation at  $\omega_s$  will build up in agreement with (11)–(14) until its amplitude is limited by some nonlinear mechanism. Suppose that the oscillation frequency deviates from  $\omega_s$  by an amount  $d\omega$ ; then the phase shift deviates from zero and the loop gain deviates from unity and its noise transfer function can be approximated as

$$\frac{S}{N}(j\omega_s + d\omega) = \frac{G(j\omega_s) + d\omega \cdot \frac{\partial G}{\partial \omega}}{1 - G(j\omega_s) - d\omega \cdot \frac{\partial G}{\partial \omega}}. \quad (20)$$

Since  $G(j\omega_s) = 1$  and, for most practical cases  $|d\omega \cdot (\partial G / \partial \omega)| \ll 1$ , (20) reduces to

$$\frac{S}{N}(j\omega_s + d\omega) = - \left( d\omega \cdot \frac{\partial G}{\partial \omega} \right)^{-1}. \quad (21)$$

This equation indicates that a noise source  $N$  is filtered by a factor  $(d\omega \cdot \partial G / \partial \omega)^{-1}$  when it appears as the oscillator signal  $S$ . The noise power spectral density of  $S$  at frequency  $\omega = \omega_s + d\omega$  is therefore given by

$$|S(j\omega_s + d\omega)|^2 = \frac{1}{d\omega^2 \cdot \left| \frac{\partial G}{\partial \omega} \right|^2} |N(j\omega_s + d\omega)|^2. \quad (22)$$

It is insightful to express the loop gain  $G$  as the product of its magnitude  $\Psi$ , and phase  $\phi$ , as  $G(j\omega) = \Psi(\omega) \exp[j\phi(\omega)]$ , at oscillation  $\Psi = 1$  and  $\phi = 0$  according to (11) and (12). Equation (22) can now be rewritten as

$$|S(j\omega_s + d\omega)|^2 = \frac{1}{4Q_{\text{loaded}}^2} \left( \frac{\omega_s}{d\omega} \right)^2 |N(j\omega_s + d\omega)|^2, \quad (23)$$

in which the general definition of the loaded quality factor  $Q_{\text{loaded}}$  is used [57]:

$$Q_{\text{loaded}} = \frac{\omega_s}{2} \sqrt{\left( \frac{\partial \Psi}{\partial \omega} \right)^2 + \left( \frac{\partial \phi}{\partial \omega} \right)^2}. \quad (24)$$

It is stressed that  $Q_{\text{loaded}}$  is not by definition equal to  $Q_{\text{unloaded}}$  as was defined by (10). However, both definitions are approximately equal when  $\omega_s \approx \omega_0$ , the impedance of the shunt capacitor satisfies  $1/\omega_0 C_s \gg R_m$ , and any resistors that are connected in series with the resonator are much smaller than  $R_m$ .

Oscillator phase noise  $\Gamma$  is approximately equal to the spectral power density  $S$  normalized to total oscillation power  $P_0$  when the phase fluctuations are much smaller than  $360^\circ$ . This condition is normally met in most cases. The total power  $P_0$  is defined as the power that is available at the node where the noise  $N$  is inserted, which is after the resonator and before the

amplifier, as defined in figure 10. Furthermore, it is assumed that only one-half of the noise in power contributes to phase noise and the other half to amplitude noise. The expression for phase noise is thus

$$\Gamma(f) = \frac{FkT}{8P_0} \frac{1}{Q_{\text{loaded}}^2} \left( \frac{f_s}{f} \right)^2, \quad (25)$$

where  $F$  represents the noise figure of the amplifier,  $k$  is Boltzmann's constant,  $T$  the absolute temperature,  $f = 2\pi \cdot d\omega$  the offset frequency from the carrier frequency, and  $f_s = 2\pi \cdot \omega_s$  representing the carrier frequency. In rewriting (23), it is furthermore assumed that the power spectral density of  $N$  is white around  $f_s$ , i.e. shows no dependence on  $f$ , and proportional to  $kT$  as will generally be the case. Note that in this expression the phase noise decreases with increasing off-set frequency  $f$  and there is no noise floor associated with the phase noise. However, in practice there will always be a noise floor that is associated with the output buffer amplifier that is required to send the signal to some external circuitry. Therefore, the complete expression for phase noise, including an expression for the noise floor caused by the output buffer, now becomes

$$\Gamma(f) = \frac{FkT}{2P_0} \left( \frac{1}{4Q_{\text{loaded}}^2} \left( \frac{f_s}{f} \right)^2 + 1 \right). \quad (26)$$

Because of the simplification, the Leeson phase-noise model provides important qualitative design insights but shows significant discrepancies from the measurement result. The Leeson model predicts boundless growth of power spectrum density at a very small offset frequency compared to that of the measured Lorentzian shape. In addition, the Leeson model only explains the  $1/f^2$  roll-off and does not explain the additional  $1/f^3$  roll-off that is observed in practical oscillators. An improvement over the cyclo-stationary Leeson's model is the cyclo-instationary Lee–Hajimiri model [58, 59]. Time variant aspects of noise injection into the oscillator loop are taken into account in the Lee–Hajimiri model. Although the general form of (26) is retained in the Lee–Hajimiri model, an additional term is added describing the  $1/f^3$  roll-off. The  $1/f^3$  term finds its origin in the upconversion of flicker noise. The Leeson and the Lee–Hajimiri models are linear, i.e. they implicitly assume that the resonator impedance is not dependent on the magnitude of the signal that is transmitted through it. However, loop gain has to be nonlinear in order to have finite oscillation amplitude after oscillation start-up, as is expressed by (14). Intentional or non-intentional nonlinearities will appear in the oscillator loop when the oscillation amplitude reaches a steady state. These nonlinearities can appear in the amplifier as well as in the resonator. For example, capacitive transduced resonators will behave nonlinear at large oscillation amplitudes, as will be shown in section 4.3. In [60, 61], it is shown that this nonlinearity can also result in upconversion of flicker noise around the carrier frequency in addition to the mechanism described by the Lee–Hajimiri model. This upconversion of flicker noise can be suppressed by limiting the oscillation amplitude by means of an automatic gain control (AGC) to relatively small values as is demonstrated in [62]. More

rigorous treatments of phase noise in MEMS oscillators including the effect of displacement-dependent stiffness and associated nonlinear resonator impedance are based on the state-space description of the oscillator loop [57]. It should be noted that for a complete analysis, not only the amplifier noise should be considered but also the noise injected via the resonator bias port [63] and mechanical noise originating from the resonator itself [64]. Despite these shortcomings of the Leeson model, several important and valid observations can be made from (26) on how to optimize a resonator in order to achieve a low phase noise.

- The near carrier as well as far from carrier noise can be reduced by increasing the input power  $P_0$  of the amplifier, i.e. minimizing the power attenuation of the resonator. This can be accomplished by reducing the motional impedance  $R_m$  of the resonator relative to impedances that are parallel to  $R_m$ .
- The input power  $P_0$  of the resonator can also be increased by driving the resonator at high power levels. Therefore, the resonator should be capable of handling high power levels.
- The phase noise close to the carrier frequency can be decreased by increasing  $Q_{\text{loaded}}$ . Therefore, the resonator should exhibit a high  $Q_{\text{unloaded}}$ , since this will typically result in a high  $Q_{\text{loaded}}$ . From (26), it is also evident that a high resonator  $Q$  will not affect the noise floor.

The above-mentioned dependences of resonator parameters  $R_m$ ,  $P_0$  and  $Q_{\text{unloaded}}$  on phase noise are also experimentally reported for several MEMS oscillators [65–67].

The phase noise of an oscillator can be manipulated by dividing or multiplying its output frequency [68, 69]. When the output frequency  $f_{s1}$  is divided down to a frequency  $f_{s2}$  the following scaling rule applies for the near-carrier noise:  $\Gamma(f)$

$$\Gamma_{f_{s2}}(f) = \Gamma_{f_{s1}}(f) \cdot \left( \frac{f_{s2}}{f_{s1}} \right)^2. \quad (27)$$

This equation shows that when two oscillators have a different oscillation frequency but identical phase noise, the oscillator with the highest frequency  $f_{s1}$  will perform better than the oscillator at the lower frequency  $f_{s2}$  when the output frequency of the high frequency oscillator is divided down to  $f_{s2}$ . In most practical cases, it is therefore beneficial to realize an oscillator at a high oscillation frequency for a good noise performance. However, high frequency resonators tend to have a lower  $Q_{\text{unloaded}}$ , as will be explained in section 4.2, which can partly offset the decrease in near-carrier noise as a result the frequency division.

Two figures of merit (FOM) are defined by (28) and (29) in order to be able to compare the noise performance of the different oscillators. Both FOMs are based on the dependences between  $f_s$  and  $P_0$  as described by (26) and (27), and can be regarded as normalized phase noise at a predefined offset frequency from the carrier frequency. FOM<sub>1</sub> corrects for differences in oscillation frequency and normalizes the noise to an oscillation frequency of 10 MHz using the relation between oscillation frequency and noise described by (27). FOM<sub>2</sub> is

based on (26) and (27) and also corrects for differences in power dissipation and normalizes the noise to an oscillator dissipating 1 mW. FOM<sub>2</sub> implicitly assumes that the ac power  $P_0$  available in the oscillating signal is linearly related to the dc dissipation  $P$  of the complete oscillator. For both FOMs, the offset frequency  $f$  is fixed at  $f = 1$  kHz at which the phase noise has not reached its floor for all oscillators considered in this review. In section 4.4, these FOMs will be used to compare the different oscillators reported in the literature:

$$\text{FOM}_1 = 10 \log (\Gamma (1 \text{ kHz})) - 20 \log \left( \frac{f_s [\text{MHz}]}{10 \text{ MHz}} \right) \quad (28)$$

$$\begin{aligned} \text{FOM}_2 = 10 \log (\Gamma (1 \text{ kHz})) - 20 \log \left( \frac{f_s [\text{MHz}]}{10 \text{ MHz}} \right) \\ + 10 \log \left( \frac{P [\text{mW}]}{1 \text{ mW}} \right). \end{aligned} \quad (29)$$

#### 4. Non-deterministic frequency stability in MEMS oscillators

In this section, an analysis is given of the parameters that set the resonator impedance level,  $Q$ -factor and power handling of piezoelectric and capacitive transduced MEMS resonators. This analysis is followed by a noise comparison of MEMS-based oscillators that have been published so far and conclusions are drawn on the limitation of the use of piezoelectric and capacitive MEMS resonators. In the last section, active transduced resonators are described as a means to overcome these limitations.

##### 4.1. Resonator impedance

The impedance  $R_m$  of the MEMS resonator should be minimized to ensure that the oscillation criteria are met and to make sure that the power attenuation of the resonator is sufficiently low to ensure that phase noise is minimized, as has been explained in sections 3.2 and 3.3. In this section, expressions for the coupling factor of capacitive and piezoelectrically transduced resonators are derived and compared. The coupling factor is an important parameter determining  $R_m$ , as is evident from (7). The coupling factor depends on its turn on resonator shape, size, resonance mode, electrode placement and bias voltage. In this review, the resonator is idealized by a lumped spring-mass system, as depicted in figure 11. For simplicity, the mass is assumed to have infinite stiffness and the spring is assumed to have no mass. For real resonators, this is obviously not the case and the mass and spring are distributed over the resonator body. However, for any resonator an effective mass and effective spring constant can be derived such that the lumped mass spring system in figure 11 applies. In order to actuate and sense the motion of the mass, the transducer can either form an integral part of the resonator, called internal transduction, or be located outside the resonating body, called external transduction. In both cases, the transducer consists of two electrodes that form a capacitor. In the case of internal transduction, the electrodes are located at either side of the



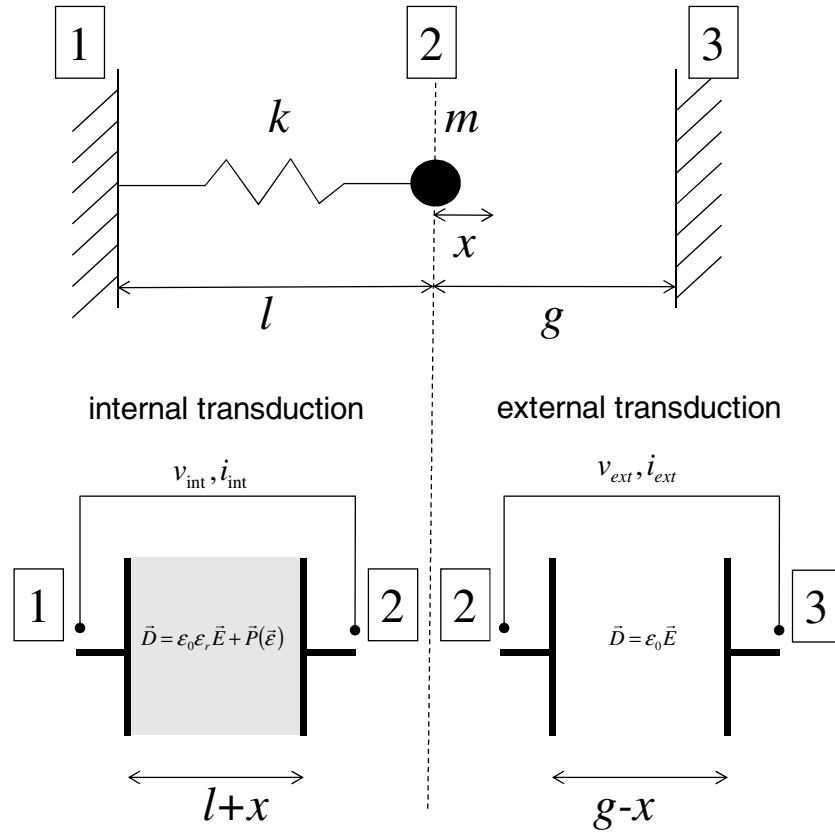


**Figure 11.** Lumped element model of a resonator (top). The transducer is either located in the resonator spring and may consist of a dielectric or piezoelectric material (internal transduction, bottom left) or located between the resonator and a fixed external electrode (external transduction, bottom right).

spring, locations 1 and 2 depicted in figure 11. The electrodes are separated by either a dielectric or piezoelectric material. For an external transducer, one of the electrodes forms an integral part of the resonator and should be located at a location where the resonator displacement is largest, i.e. near the resonator mass indicated by location 2 in figure 11. The other electrode is put in close proximity to the first one, but is located outside the resonator and is fixed in position, as is indicated by location 3 in figure 11. For an external transducer, the two electrodes are mechanically decoupled and the transducer does not contribute to the spring constant of the resonator. Therefore, the space between the two electrodes needs to be mechanically compliant and is therefore typically left empty or filled with a gas. In principle, also a liquid can be used as is reported in [70].

The coupling factor as defined by (2) and (3) can now be derived by considering the electrical charge on electrodes 1, 2 and 3 as a function of resonator displacement  $x$ . In general, the electric displacement field  $\vec{D}$  is related to the applied electric field  $\vec{E}$  and the polarization field  $\vec{P}$  by the following relation [9]:

$$\vec{D} = \epsilon_0 \vec{E} + \vec{P}(\vec{E}, \vec{\epsilon}), \quad (30)$$

where the polarization is a function of the applied field and, for a piezoelectric material, is also dependent on the mechanical strain field  $\epsilon$  that is present in the piezoelectric layer. Piezoelectric materials are anisotropic in nature.

Therefore, the functional dependence between the polarization field and mechanical strain is described by a tensor  $e_{ij}$ . For most piezoelectric materials, also non-zero matrix elements  $e_{ij}$  with  $i \neq j$  exist. In some case, e.g. for quartz, these off-axis elements can even be larger than the  $e_{ii}$  elements. In these cases, the direction of the electric field-induced strain does not coincide with the direction of the polarization field. This is also the reason that the commonly used AT cut quartz crystals resonate in a direction perpendicular to the direction of the applied electric field [51]. These tensor operations are typically very tedious and do not always lead to an intuitive end result. For this reason, the resonator depicted in figure 11 is assumed to be one-dimensional with only one degree of freedom  $x$ . Strains and stresses in directions other than the  $x$ -direction are assumed to be zero. By doing so, the relation between the polarization and applied electric field is given by a simple scalar multiplication factor  $\epsilon_0(\epsilon_r - 1)$ , with  $\epsilon_r$  the material's relative permittivity, and tedious tensor analysis is avoided. In the case of a piezoelectric material, the strain dependence is now described by a simple scalar multiplication factor  $e_{xx}$ . The electric displacement in the  $x$ -direction for the internal and external transducer can now simply be written as

$$D_{x,\text{int}} = \epsilon_0 \epsilon_r \frac{V + v_{\text{int}}}{l + x} + e_{xx} \frac{x}{l} \quad (31)$$

$$D_{x,\text{ext}} = \epsilon_0 \frac{V + v_{\text{ext}}}{g - x}, \quad (32)$$

where the applied electric field is written as  $E_{x,int} = (V + v_{int})/(l + x)$  and  $E_{x,ext} = (V + v_{ext})/(g - x)$  for internal and external transduction, respectively. In (31), the one-dimensional strain is defined as  $\varepsilon_x = x/l$ . The currents  $i_{int}$  and  $i_{ext}$  can now be derived from (31) and (32) by taking the time derivative of  $D$  and multiplying it by the electrode area  $A$ :

$$i = A \frac{\partial D_x}{\partial t}. \quad (33)$$

The output current for the internal transducer can now be approximated as in (34), assuming that the displacement  $x$  is much smaller than  $l$  and  $g$ , and also assuming that  $v_{int}$  and  $v_{ext}$  are much smaller than the bias voltage  $V$ :

$$i_{int} \approx C_{int} \frac{\partial v_{int}}{\partial t} - (\eta_{int,cap} - \eta_{int,piezo}) \frac{\partial x}{\partial t}, \quad (34)$$

with

$$\eta_{int,cap} = V \frac{\varepsilon_0 \varepsilon_r A_{int}}{l^2} \quad (35)$$

$$\eta_{int,piezo} = \frac{e_{xx} A_{int}}{l} \quad (36)$$

$$C_{int} = \frac{\varepsilon_0 \varepsilon_r A_{int}}{l}. \quad (37)$$

Two electro-mechanical coupling factors  $\eta_{int,cap}$  and  $\eta_{int,piezo}$  arise from this analysis. The capacitive coupling factor  $\eta_{int,cap}$  results from the varying capacitance between electrodes 1 and 2 as a result of the displacement  $x$  of the electrodes. The piezoelectric coupling factor  $\eta_{int,piezo}$  is a result of the strain-induced variation of polarization. For a non-piezoelectric internal transducer,  $\eta_{int,piezo} = 0$ . The  $C_{int}$  is simply the nominal capacitance between electrodes 1 and 2.

The most common electrode configurations for an external transducer are the ‘parallel plate’ and the ‘interdigital’ configuration [9]. The parallel plate transducer exhibits the strongest change of capacitance per unit of resonator displacement for a given transduction gap and therefore exhibits the largest coupling factor and lowest impedance and therefore will be analyzed below. Using the same assumptions as were used for deriving the expression for  $i_{int}$ , the output current for an external parallel plate transducer  $i_{ext}$  can be written as

$$i_{ext} \approx C_{ext} \frac{\partial v_{ext}}{\partial t} + \eta_{ext,cap} \frac{\partial x}{\partial t}, \quad (38)$$

with

$$\eta_{ext,cap} = V \frac{\varepsilon_0 A_{ext}}{g^2} \quad (39)$$

$$C_{ext} = \frac{\varepsilon_0 A_{ext}}{g}. \quad (40)$$

The coupling factor  $\eta_{ext,cap}$  results from the varying capacitance between electrodes 2 and 3 as a result of the displacement  $x$  of the electrodes. The  $C_{ext}$  is simply the nominal capacitance between electrodes 2 and 3 and constitutes, just as  $C_{int}$ , part of the total capacitance  $C_s$  between the two resonator terminals. The difference between  $\eta_{ext,cap}$  and  $\eta_{int,cap}$  is that the displacement  $x$  is relative to  $g$  in  $\eta_{ext,cap}$

and to  $l$  in  $\eta_{int,cap}$ . Furthermore, internal transduction allows for a  $\varepsilon_r > 1$ , since the space between electrodes can be filled with a solid with a high dielectric constant.

The coupling factors  $\eta_{int,piezo}$ ,  $\eta_{ext,cap}$  and  $\eta_{int,cap}$  relate the different types of transduction reported in the literature to the resonator impedance by means of (7). Given the mode shape and size of the resonator, the coupling factor should be maximized through proper transducer placement in order to obtain as small as possible impedance at resonance. An important observation is that the expressions for  $\eta_{int,piezo}$ ,  $\eta_{ext,cap}$  and  $\eta_{int,cap}$  show that a decrease in electrode area, as may be required for reasons of miniaturization, decreases the coupling factor and thus leads to an increase in resonator impedance  $R_m$ . This ultimately sets limits to minimum resonator size that is required for meeting the oscillation condition and phase noise requirements as was described in sections 3.2 and 3.3 and is as such a fundamental limitation of the application of these transduction methods to microresonators. In the following, a comparison between the three coupling factors  $\eta_{int,piezo}$ ,  $\eta_{ext,cap}$  and  $\eta_{int,cap}$  is made.

In the case of piezoelectric transduced resonators, the transducer element consists of a thin film onto which metallic electrodes are deposited near locations of maximum strain. Often the transducer element and resonator body are identical as is the case in FBAR and BAW resonators where a standing wave is excited inside the piezoelectric film. The piezoelectric material that is used in MEMS resonators is almost exclusively PVD AlN [53, 71–76], but sometimes other materials such as ZnO [77] are used as well. An important disadvantage of AlN-based resonators is that the  $Q$ -factors that can be obtained are relatively low. The low  $Q$ -factor seems to be a result of material losses associated with the metal electrodes that need to be deposited onto the AlN as will be elaborated in section 4.2. For almost all capacitive transduced resonators, Si is used for the resonator body and in many cases the resonator is processed on a silicon-on-insulator (SOI) substrate. In some cases, especially when the resonator needs to be deposited at low temperature, capacitive transduced resonators are made from alternative materials, such as electroplated Ni [48], PECVD SiGe [45] or polycrystalline diamond [78]. Very high  $Q$ -factor can be obtained with capacitive transduced resonators, since no lossy metallic electrodes need to be deposited on top of the resonator as is the case for piezoelectric transduced resonators, see also section 4.2.

The coupling factor for a piezoelectric resonator is given by the difference of the capacitive coupling factor  $\eta_{int,cap}$  and piezoelectric coupling  $\eta_{int,piezo}$  as is described by (34). However, the  $\eta_{int,piezo}$  is typically much larger in magnitude than  $\eta_{int,cap}$  as is illustrated by considering the ratio of the piezoelectric and capacitive coupling factor:

$$\frac{\eta_{int,piezo}}{\eta_{int,cap}} = \frac{l}{V} \frac{e_{33}}{\varepsilon_0 \varepsilon_r}. \quad (41)$$

Assume that a 1  $\mu\text{m}$  thick AlN film that is biased at 5 V and in which the strain is uniformly distributed along its  $c$ -axis than the piezoelectric coupling factor is more than three orders of magnitude larger than the capacitive coupling factor, as is shown in table 2. Therefore, piezoelectric resonators

**Table 2.** Comparison of piezoelectric and capacitive coupling constant for a 1  $\mu\text{m}$  thick AlN layer that is biased at 5 V. Material parameters are taken from [83, 84].

Material	$e_{33}$ (C m <sup>-2</sup> )	$\epsilon_r$	V (V)	$l$ (m)	$\eta_{\text{piezo}}/\eta_{\text{cap}}$
AlN	1.55	10.4	5.0	1.0E-06	3.2E+03

tend to have lower impedance. The capacitive coupling factor decreases more rapidly than the piezoelectric coupling factor when the effective spring length  $l$  is made smaller, as is evident from (41). The effective spring length of any resonator is related to its frequency; short springs will result in a resonator with high stiffness and corresponding high resonance frequency. Therefore, the difference in coupling factor between capacitive and piezoelectric transduction tends to decrease when the resonance frequency increases. Several examples exist of internally capacitive transduced Si resonators where the electrodes are separated by an embedded dielectric layer [79, 80] or by a depletion layer that is created inside the silicon [81, 82]. Although the coupling factor for internally transduced capacitive resonators is typically lower than for piezoelectric transduced resonators, the Si-based resonator tends to have a higher  $Q$ -factor (see section 4.2), which partly off-sets the low coupling factor for achieving a low impedance at resonance.

For an externally transduced resonator, the electrode is separated from the resonating body by an air gap  $g$ . This air gap is not related to the stiffness and resonance frequency of the resonator, as is the case for internally transduced capacitive resonators. Consequently, externally transduced capacitive resonators can exhibit a higher coupling factor and thus lower impedance than their internal transduced counterparts when the resonance frequency is relatively low [85–87]. In order to get a high  $\eta_{\text{ext, cap}}$ , several parameters can be optimized as can be seen from (39). The bias voltage  $V$  should be as large as possible, but is often limited by circuit limitations to values below 10 V. Alternatively, also a build-in charge can be used to create a polarization field over the gap [88]. The most straightforward and effective way of increasing the coupling factor is to decrease the transduction gap, because of the  $g^2$  dependence described in (39). Therefore many approaches have been investigated for the processing of narrow transduction gaps and are described in [89–100]. Another approach for increasing the coupling factor is to increase the total electrode area by operating several identical resonators in parallel as is reported in [66]. The overall coupling factor that can also be increased through a combination of capacitive and piezoelectric transduction is described in [101].

In tables 3 and 4, we give the impedance at resonance, resonance frequency and  $Q$  factor for a large variety of piezoelectric and capacitive transduced resonators published in the literature. Table 3 gives the overview for piezoelectric resonators. Table 4 gives the overview for capacitive resonators and also mentions the transduction gap and bias voltage. Figures 12(a) and (b) are constructed from these tables. In figure 12(a), the impedance versus frequency is plotted for the piezoelectric and capacitive resonator. In figure 12(b), the impedance is normalized to resonator  $Q$  in

**Table 3.** Literature overview of resonance frequency, resonance mode,  $Q$ -factor and impedance of piezoelectric resonators.

Reference	Center frequency (Hz)	$Q$ -factor	Mode	$R_m$ ( $\Omega$ )
[105]	9.66E+05	140 000	AlN on Si bulk	2.00E+02
[72]	1.70E+06	6200	ZnO on Si flex	
[74]	1.44E+07	2300	AlN bulk	3.76E+02
[75]	1.96E+07	786	AlN bulk	8.12E+03
[75]	7.88E+07	1061	AlN bulk	7.90E+02
[75]	1.02E+08	1257	AlN bulk	1.14E+03
[77]	1.06E+08	4000	AlN on Si bulk	2.50E+02
[106]	1.76E+08	1500	AlN bulk	7.10E+01
[108]	2.08E+08	6100	AlN on Si bulk	7.00E+01
[106]	2.22E+08	2100	AlN bulk	3.50E+01
[53]	2.23E+08	2100	AlN bulk	3.50E+01
[106]	3.07E+08	1400	AlN bulk	2.60E+01
[109]	4.27E+08	1400	AlN on Si bulk	1.80E+02
[110]	4.67E+08	1850	ZnO + c-C + SiO <sub>2</sub>	6.00E+02
[106]	4.82E+08	850	AlN bulk	9.20E+01
[111]	4.96E+08	3800	AlN on Si bulk	6.00E+02
[112]	6.00E+08	2000	AlN bulk	
[113]	1.01E+09	7100	AlN on Si bulk	1.50E+02
[73]	2.00E+09	700	AlN bulk	3.00E+01

order to have a more objective comparison of the coupling factor-induced difference in  $R_m$ . From these figures, it can be seen that capacitive resonators exhibit larger impedance than piezoelectric resonators. Furthermore, externally transduced capacitive resonators do not show a clear frequency dependence, while the impedance of piezoelectric resonators tends to decrease with increasing resonance frequency. All these observations are in line with the foregoing analysis. The large variation in the reported impedance of capacitive resonators can be attributed to geometric factors, such as a difference in gap width and electrode area, as well as variations in the applied bias voltage.

It should be stressed that the value of the resonator impedance  $R_m$  should be low in comparison with other impedance levels that connect to the resonator terminals. Therefore, the value of the coupling factor should be seen in relation to this. For example, in order to meet the oscillation criterion for loop phase, the resonator impedance should be as low as possible in relation with the impedance of the shunt capacitor  $C_s$ , as is described in (17). For an externally transduced capacitive resonator  $R_m$  is to a first order insensitive to frequency scaling and the shunt impedance caused by  $C_{\text{ext}}$  decreases with frequency when the gap width and electrode areas remain fixed. Therefore, it is challenging to meet the oscillation condition for capacitive resonator at high frequencies. However, an alternative approach for meeting the oscillation condition is to minimize shunt capacitance  $C_s$  instead of  $R_m$ . The suppression of  $C_{\text{ext}}$  is an important design approach to meet the oscillation condition for externally transduced capacitive resonators. A method for suppressing  $C_{\text{ext}}$  is driving the resonator over a different gap than the gap that is used for sensing, as is shown in figure 13. In this way, the gap capacitance  $C_{\text{ext}}$  is shorted to ground and does not add to the shunt capacitance  $C_s$ . A drawback of this technique is that for obtaining the same motional impedance twice the electrode

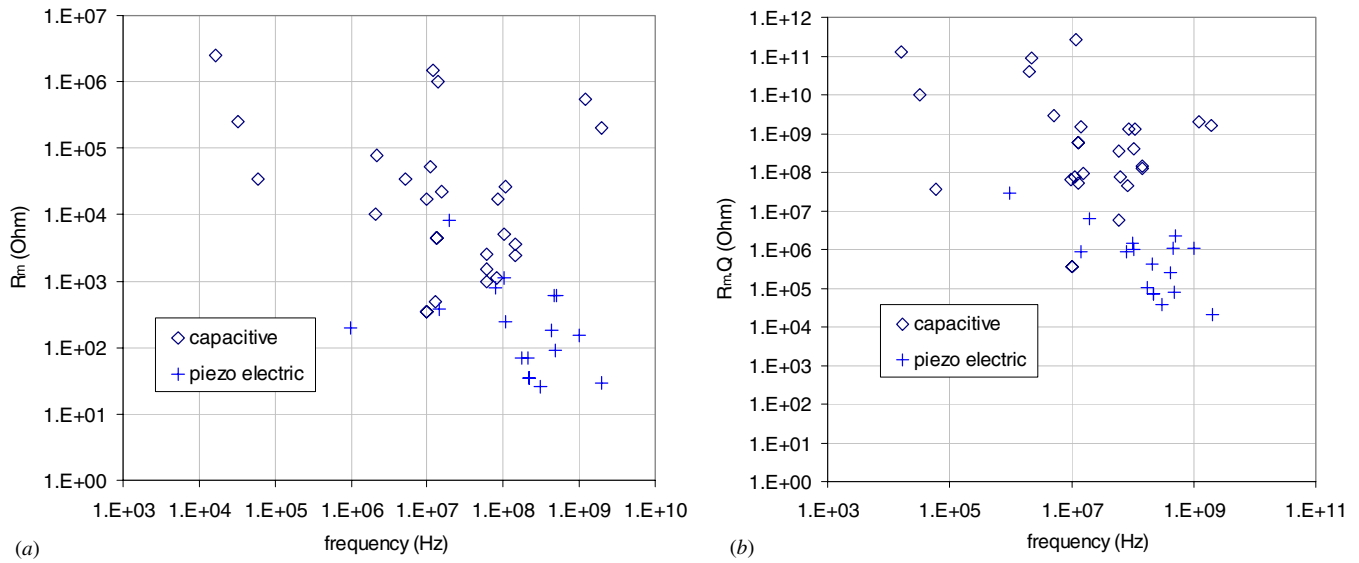


**Figure 12.** (a) Overview of reported motional resistance  $R_m$  versus resonance frequency for capacitive and piezoelectric resonators. (b) Same overview as depicted in (a) but  $R_m$  is now normalized to  $Q$  in order to better compare coupling factors.

**Table 4.** Literature overview of resonance frequency, resonance mode,  $Q$ -factor, gap width, impedance, bias voltage and transducer gap width of capacitive resonators.

Reference	Center frequency (Hz)	$Q$ -factor	Mode	$R_m$ ( $\Omega$ )	Bias voltage (V)	Resonator gap (nm)
[114]	1.65E+04	51 000	Si flex	2.50E+06	32	2000
[115]	3.20E+04	40 000	Si flex	2.50E+05	3	1000
[55]	6.00E+04	1000	Si flex	3.50E+04	28	1000
[116]	1.00E+06		Si flex		7	
[117]	2.06E+06	4050 000	Si bulk	1.00E+04	50	2000
[104]	2.18E+06	1160 000	Si bulk	7.64E+04	60	3000
[118]	5.10E+06	80 000	Si flex	3.50E+04	5	400
[119]	5.40E+06	2020 000	Si bulk			2000
[120]	6.30E+06	1600 000	Si bulk			2000
[121]	9.75E+06	3600	Si flex	1.75E+04	7	100
[62]	1.00E+07	1036	Si flex	3.40E+02	13	100
[62]	1.00E+07	1036	Si flex	3.40E+02	13	100
[122]	1.20E+07	180 000	Si bulk	1.50E+06	100	1000
[123]	1.30E+07	100 000	Si bulk	5.00E+02	20	180
[124]	1.31E+07	130 000	Si bulk	4.47E+03	100	750
[125]	1.31E+07	130 000	Si bulk	4.47E+03	100	750
[126]	1.40E+07	1500	Si flex	1.00E+06	130	1000
[66]	1.54E+07	4360	Si flex	2.20E+04	30	300
[47]	1.9E+07	220 000	Si torsion	1.2E+04	1	130
[127]	2.40E+07	53 000	Si bulk	2.10E+03	5	110
[67]	5.99E+07	6200	Si bulk	9.66E+02	16	32
[67]	6.10E+07	130 000	Si bulk	2.60E+03	16	92
[128]	6.12E+07	48 000	Si bulk	1.50E+03	12	80
[129]	8.12E+07	40 000	Si bulk	1.10E+03	10	65
[129]	8.59E+07	77 000	Si bulk	1.71E+04	7	170
[130]	1.03E+08	80 000	Si bulk	5.00E+03	18	200
[129]	1.07E+08	49 600	Si bulk	2.65E+04	10	170
[129]	1.44E+08	39 000	Si bulk	3.60E+03	50	135
[131]	1.45E+08	51 000	Si bulk	2.40E+03	14	77
[132]	1.20E+09	3700	Si bulk	5.60E+05	20	85
[79]	1.90E+09	1400	AlN bulk			
[133]	1.95E+09	8000	Si bulk	2.00E+05	20	
[86]	4.50E+09	11 000	Si bulk			

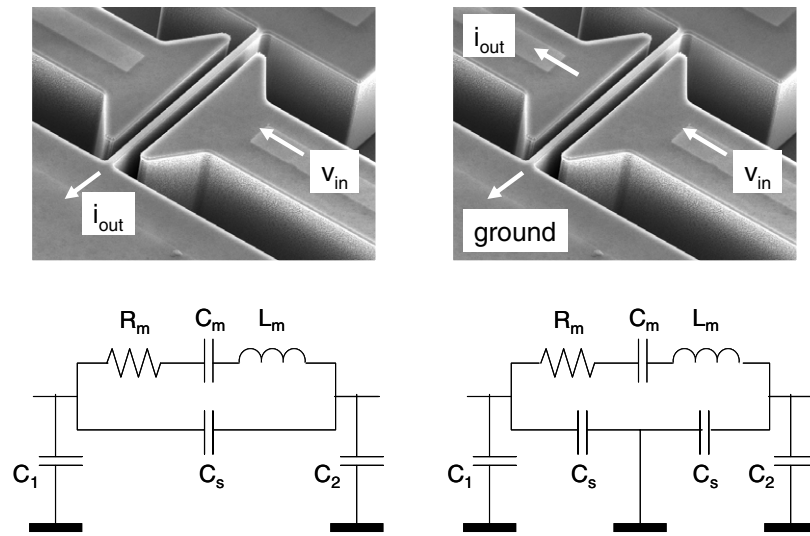


**Figure 13.** Top-left: top view of a clamped–clamped resonator including electrical terminals using a single transduction gap. Top-right: topview of a clamped–clamped resonator including electrical terminals using a double transduction gap. Bottom-left:  $C_s$  is part of the transmitted signal for a single gap device. Bottom-right:  $C_s$  is grounded in a dual gap device and added to  $C_{1,2}$ .

area is required, since one electrode is only used for driving the resonator and a second electrode is only used for sensing. Other techniques for suppressing the shunt impedance include balancing or frequency-doubling techniques, as is described in [102–104].

#### 4.2. $Q$ -factor

There are many reasons to aim for a high resonator  $Q$ -factor, as is explained in the previous sections. High resonator  $Q$ -factors result in low resonator impedance, since  $R_m$  is inversely proportional to  $Q$ . Low resonator impedance is required to meet oscillation conditions, as is expressed by (17). High  $Q$ -factors will also result in a low phase noise close to carrier, as is expressed by (26). Furthermore, high- $Q$  resonators are required for good frequency stability of the oscillator that is not affected by e.g. bias or temperature drift induced by the sustaining amplifier.

The physical quality factor  $Q_{\text{unloaded}}$  is defined as the ratio of the energy that is stored in the resonator and the energy that is lost in one cycle and can be expressed as in (10). Energy loss can be attributed to several loss mechanisms. Loss factors can either be external: energy leaves the resonator and is dissipated outside of the resonator, or internal: mechanical energy is directly dissipated inside or at the surface of the resonator [144]. A classification of different loss mechanisms is depicted in figure 14. The  $Q_i$  associated with a specific loss mechanism is related to the overall resonator  $Q$  through the following relation:

$$\frac{1}{Q} = \sum_i \frac{1}{Q_i}. \quad (42)$$

External loss can be caused by electrical loading of the resonator as can easily be understood considering the equivalent electrical model of the resonator. When an external

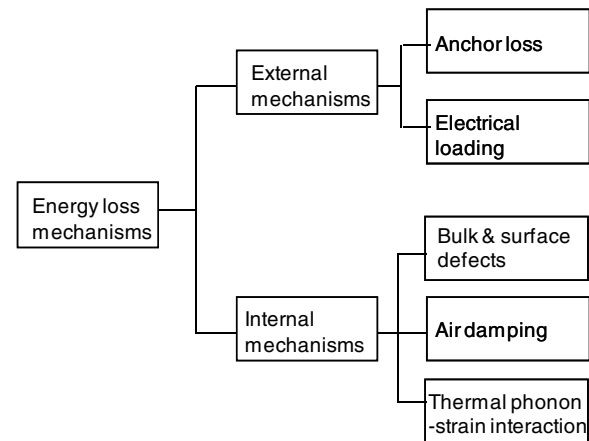


**Figure 14.** Classification of loss mechanisms in a mechanical resonator.

resistor is connected in series with the resonator, the total resistance at resonance is given by  $R = R_{\text{load}} + R_m$ . The electrical current that is flowing through the resonator is also flowing through  $R_{\text{load}}$  causing additional power dissipation and a lowering of the  $Q$ -factor as a result. The lowering of  $Q$  due to electrical loading can be avoided by choosing  $R_{\text{load}} \ll R_m$ . External losses do also occur in the mechanical domain. Acoustic energy is not perfectly reflected at the resonator's boundaries but can radiate into the supporting substrate, lowering the resonator  $Q$ . This loss mechanism is often called 'anchor loss'. Several design approaches can be used for suppressing anchor loss. Some are based on material mismatch, i.e. creating a resonator interface out of materials with different acoustic impedance [145]. Other designs are based on carefully positioning the anchors exactly at nodes of the resonance mode. Furthermore, the shape of the anchor can be tailored such that it supports a quarter wavelength



at resonance thereby increasing the acoustic reflection at the anchor end [146].

Gas damping can be classified as squeeze film and shear damping [147]. Squeeze film damping is especially present in the transduction gap of capacitive resonators and is absent in piezoelectric resonators. In [148], it is shown that the squeeze film damping is prominent below a certain turn-over frequency. Below this frequency, the gas molecules are sucked in and out of the gap when the resonator moves thereby causing a dissipative damping force on the resonator. Above the turn-over frequency, the inertia of the gas molecules is too large to follow the movement of the resonator and their presence acts as an air cushion on the resonator adding to the spring constant of the resonator and thereby slightly raising its frequency. At atmospheric pressure and below 1 GHz, gas damping is generally the loss mechanism that dominates the overall resonator  $Q$  for capacitive MEMS resonators. The  $Q$ -factor that is set by gas damping is frequency and mass dependent irrespective of whether squeeze film or shear damping is the underlying damping mechanism. This can be understood by combining (8) and (10) into (43).  $Q_{\text{unloaded}}$  can be expressed as a function of resonance frequency  $\omega_0$  and a characteristic resonator dimension  $l$  by appreciating the fact that the damping loss scales with resonator area, thus with  $l^2$ , and resonator mass scales with resonator volume, thus with  $l^3$ :

$$Q_{\text{unloaded}} = \frac{\omega_0 m}{\gamma} \sim \omega_0 l. \quad (43)$$

This expression shows that when a resonator is miniaturized, i.e. when  $l$  is decreased, while its resonance frequency is kept constant it will exhibit a lower  $Q$ . This is a direct result of the fact that the energy stored in the resonator is reduced more than the energy dissipation caused by air damping. For the same reason, the  $Q$ -factor is further reduced when the resonator is not only miniaturized, but also lowered in resonance frequency. Therefore, the  $Q$ -factor of a small and low frequency resonator suffers most from air damping. In figure 15, the  $Q$ -factor is measured as a function of ambient pressure for a 32 kHz [115] and a 55 MHz resonator. It can be seen that the  $Q$ -factor of the 32 kHz resonator is much more sensitive to air damping. Special care should be taken to maintain a low gas pressure inside the resonator package in order not to limit the overall resonator  $Q$ , as was mentioned in section 2. It can be seen that in this case the 32 kHz requires a cavity pressure below 0.01 mbar in order not to limit its  $Q$ -factor by air damping, while the 55 MHz MEMS resonator can tolerate up to 10 mbar before air damping starts to dominate its overall  $Q$ -factor.

Bulk and surface conditions have shown to impact the  $Q$  factor. Several research groups have experimentally observed that the  $Q$  values decrease as surface-to-volume ratios increase. In particular, the  $Q$ -factor of very thin cantilevers has been found to scale linearly with resonator thickness [149]. Also coating the resonator with a thin film, e.g. using atomic layer deposition (ALD), has shown to result in a considerable decrease of resonator  $Q$  [67], indicating interface-induced losses. Furthermore, flexure mode resonators typically have lower  $Q$  than the bulk mode resonator. This is a further indication that acoustic energy is most dominantly lost at the resonator surface rather than in its interior, since for the

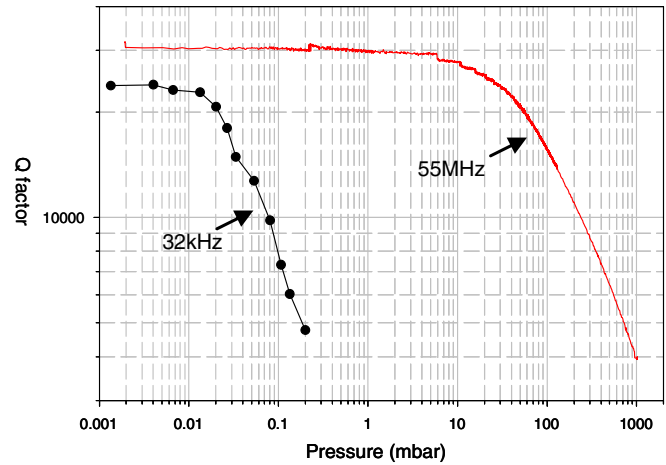


**Figure 15.** Pressure dependence of the unloaded  $Q$ -factor for a 32 kHz and a 55 MHz capacitive MEMS resonator. The 32 kHz capacitive MEMS resonator requires a cavity pressure below 0.01 mbar in order not to limit its  $Q$ -factor by air damping, while the capacitive 55 MHz MEMS resonator can tolerate up to 10 mbar before air damping starts to limit the  $Q$ -factor.

flexural mode resonator the acoustic energy concentrates near the surface while for bulk resonators the acoustic energy is uniformly distributed over its interior.

A fundamental thermodynamical limitation of the resonator  $Q$  is due to the interaction between thermal phonons and the mechanical strain field inside the resonator caused by its motion [150–152]. The strain field inside the resonator leads to a non-equilibrium distribution of the thermal phonons. As a result, the phonon distribution tends to restore to thermal equilibrium, which causes an increase of entropy and hence a reduction of  $Q$ . Although several types of phonon interaction can be distinguished, all types predict that the product of resonance frequency and  $Q$ -factor is bound to an upper limit for resonance frequencies  $< 1$  GHz. The predicted maximum obtainable  $f \cdot Q$  product lies between  $2.5 \times 10^{13}$  Hz and  $3.9 \times 10^{13}$  Hz for Si and between  $9 \times 10^{12}$  and  $2.5 \times 10^{13}$  Hz for AlN. For quartz, this limit is predicted to be between  $1.8 \times 10^{13}$  Hz [153] and  $3.2 \times 10^{13}$  Hz indicating that maximum  $Q$  factors obtainable with MEMS are of the same order of magnitude to what can be obtained with quartz. It is also predicted that the  $f \cdot Q$  product exhibits a strong temperature dependence [154]. The increase of  $Q$  at cryogenic temperatures has also been observed experimentally [155–158].

In figure 16, the  $Q$ -factor is plotted for a large variety of resonators reported in the literature [117, 119, 120, 132, 133, 146, 159, 160]. All data points are measured under such conditions that gas damping is not dominating the overall  $Q$ -factor. The predicted maximum obtainable  $fQ$  product is resembled by the dashed line for AlN, quartz and Si, respectively. Very high  $Q$ -factors approaching the theoretical limit are obtained for bulk mode Si resonators. In bulk mode resonators, the resonating body is stretched and compressed in a longitudinal fashion and the mechanical stress and strain are evenly distributed over the body interior. In contrast, flexural mode Si resonators show a relatively low  $Q$ -factor which might be caused by the fact that in a flexural mode resonator, the stress and strain are mostly located at the (lossy) resonator surface.

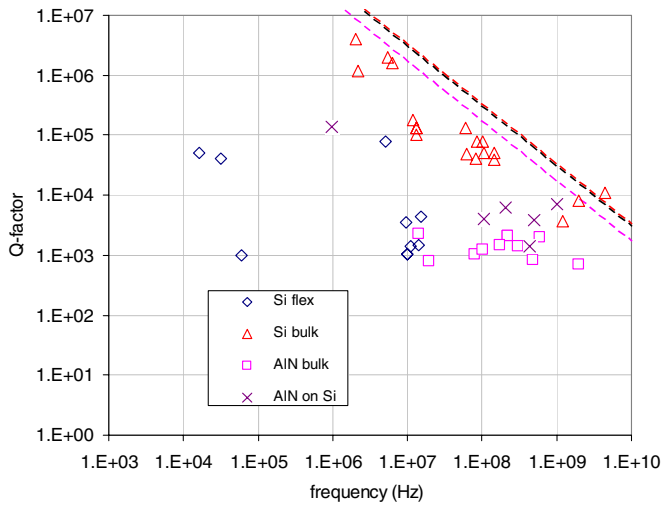


**Figure 16.** Overview of reported values of the unloaded  $Q$ -factor versus resonance frequency. The predicted maximum obtainable  $f$ - $Q$  product is resembled by the dashed line for AlN (purple), quartz (black) and Si (red), respectively. Data are taken from table 5.

AlN-based bulk mode piezoelectric resonators show a lower  $Q$  than bulk mode Si resonators [53, 72–74, 76] and reported values are well below the theoretical  $f$ - $Q$  limit especially for lower frequencies. The lower than expected  $Q$ -factor of AlN-based resonators can be explained by losses associated with the metal electrode that is deposited on the AlN needed for driving the resonator [161, 162]. Also data points are shown in figure 16 for Si bulk mode resonators that are coated with a AlN layer [77, 105, 109, 111, 113]. It can be seen that the  $Q$ -factor of this type is somewhere between bulk mode Si resonators and AlN-based resonators.

#### 4.3. Power handling and large signal behavior

The analysis so far has been limited to a linear description of the resonator and oscillator, i.e. couplings factors  $\eta_{\text{int,piezo}}$ ,  $\eta_{\text{ext,cap}}$  and  $\eta_{\text{int,cap}}$ , and spring constant  $k$  do not depend on the ac voltage that is being applied to the resonator. This description is only valid when the resonator amplitude  $x$  is small compared to the spring length  $l$  and gap width  $g$ . However, it is beneficial to have an as large as possible ac swing in the oscillator loop so as to maximize the power  $P_0$  and to minimize phase noise, as can be seen from (26). Therefore, the resonator should be operated close or into the nonlinear regime and the amplitude at resonance should be maximized for best noise performance.

Several causes of resonator nonlinearity can be identified and some are specific for capacitive resonators [60, 134–136]. Generic nonlinearities that apply to all mechanical resonators are related to material properties of the resonating medium [137]. An ideal material shows a linear relation between stress and strain, but for large stress and strain levels this relation starts to deviate from a straight line and the resonator's stiffness becomes dependent on stress and strain. Furthermore, it can be expected that piezoelectric coefficients will exhibit nonlinear behavior at such high strain levels [138] which do not play a role in capacitive transduction. On the other hand,

some nonlinearities are specific to capacitive transduction and are a direct cause of the nonlinear relation between gap capacitance and displacement, as is illustrated below for an external capacitive transducer. The force  $F_x$  between the two electrodes can be derived by taking the gradient of the stored energy followed by a Taylor expansion in  $x$ :

$$\begin{aligned} F_x &= -\frac{\partial E}{\partial x} = -\frac{1}{2}V^2\frac{\partial C}{\partial x} \\ &= -\left(\frac{1}{2}V_{dc}^2 + v_{ac}V_{dc} + \frac{1}{2}v_{ac}^2\right)\frac{\varepsilon_0 A}{(g-x)^2} \\ F_x &= -\frac{\varepsilon_0 AV_{dc}}{g^2}\left(V_{dc}\frac{x}{g} + 2V_{dc}\frac{x^2}{g^2} + 2v_{ac}\frac{x}{g} + \dots\right). \end{aligned} \quad (44)$$

The first term in this equation is a force that is independent on the ac component of the voltage, but is dependent on the resonator displacement and can therefore be considered a spring force. This term adds to the mechanical spring force, which is typically much higher in value, and can be used to fine tune the mechanical resonance frequency e.g. to compensate for its temperature dependence, as will be explained in section 5.1. The second term can also be considered a spring force, but with a spring constant that depends on  $x$ . This implies that according to (6) and (8), the motional capacitance  $C_m$  and resonance frequency  $\omega_0$  are functions of the resonator amplitude  $x$ . In [138] it is shown that this term can increase  $Q_{\text{loaded}}$ , as defined by (24), and can be expected to decrease the near-carrier phase noise, as can be deduced from (25). For a piezoelectric resonator, it has indeed been demonstrated that the  $x$  dependence of the spring constant can improve phase noise by up to 20 dB [139]. The third term in (44) comprises the product of two time-varying signals:  $v_{ac}$  and  $x$ . If the resonator is excited by a noisy voltage  $v_{ac} + v_n$ , where  $v_n$  represents the noise term, then the product  $x \cdot (v_{ac} + v_n)$  contained in the third term will result in upconversion of the  $v_n$  spectrum around the oscillation frequency. This mechanism can result in the upconversion of flicker noise in the oscillator loop leading to a  $1/f^3$  instead of a  $1/f^2$  of the near-carrier noise roll-off thereby causing a deterioration of the near-carrier phase noise [60]. This simple analysis shows that different nonlinearities in the resonator can result in an improvement as well as a deterioration of the near-carrier noise.

Other than material or transduction nonlinearities, it is also possible that mechanical instabilities occur in the resonator when driven at high power levels. It is shown in [76, 140] that high power levels can cause mode coupling inside the resonator. In [141–143], it is described that a resonator that is driven in-plane can start resonating out-of-plane at increased power levels. The excitation of parasitic modes causes an energy leak of the resonance mode that is supported in the oscillator loop and poses an upper limit to the amplitude  $x$  and hence the oscillating power  $P_0$ . This results in a limit of the achievable phase noise performance, as is obvious from (26).

#### 4.4. Noise comparison

In this section, an overview is given of the performance of MEMS oscillators that have been reported in the literature to date. The data are grouped in capacitive and piezoelectric

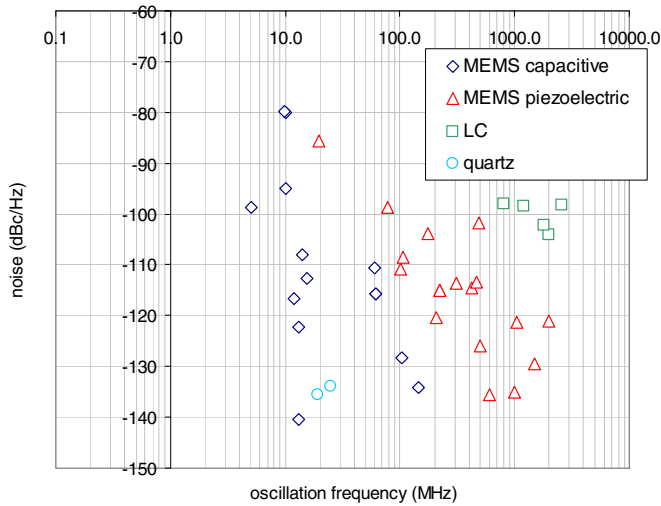


**Figure 17.** Phase noise at 1 kHz offset normalized to an oscillation frequency of 10 MHz,  $FOM_1$  as a function of oscillation frequency for capacitively and piezoelectrically transduced oscillators. For comparison also the  $FOM_1$  for LC-based electrical oscillators are included, as well as the  $FOM_1$  for quartz-based oscillators.

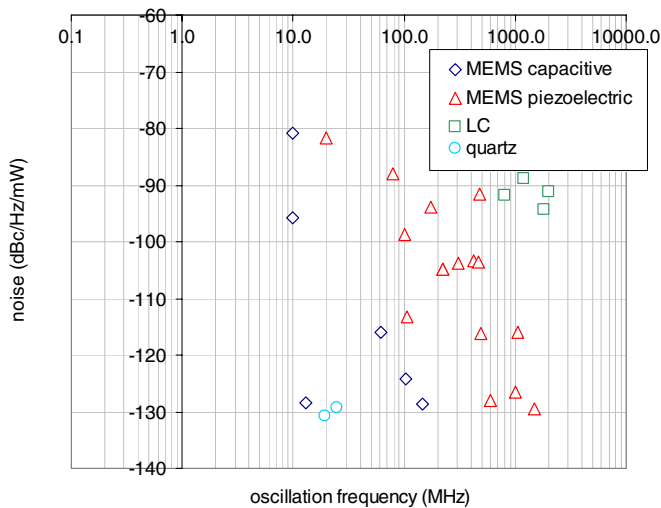


**Figure 18.** Phase noise at 1 kHz offset normalized to an oscillation frequency of 10 MHz and power dissipation of 1 mW,  $FOM_2$  as a function of oscillation frequency for capacitive and piezoelectric transduced oscillators. For comparison also the  $FOM_2$  for LC-based electrical oscillators are included, as well as the  $FOM_2$  for quartz-based oscillators.

oscillators. Furthermore, several quartz oscillator [118, 163] and LC-based oscillators [164–167] are included for comparison. The most important parameters are depicted in tables 5 and 6. It is interesting to see that most MEMS oscillators exhibit  $1/f^3$  near carrier roll-off indicating the presence of upconversion of flicker noise in the oscillator loop, as is explained in section 3.3. In figures 17 and 18, an overview of the  $FOM_1$  and  $FOM_2$  is plotted. It can be seen that there is a trend of decreasing noise with increasing oscillation frequency regardless of the type of transduction being used. Furthermore, at a fixed oscillation frequency, it can be seen that quartz oscillators exhibit lowest  $FOM_1$  and  $FOM_2$ , followed by capacitive, piezoelectric and LC

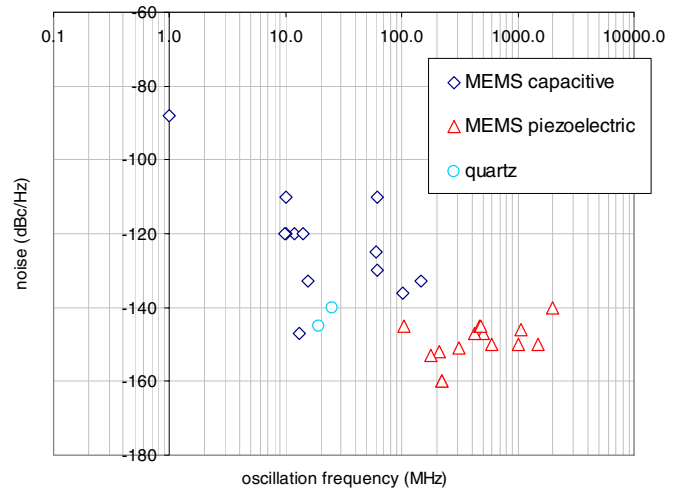


**Figure 19.** Noise floor as a function of oscillation frequency for capacitive and piezoelectric transduced oscillators. For comparison also the noise floor for quartz oscillators is included.

oscillators. The superior quartz performance can be explained by the fact that quartz resonators exhibit a high  $Q$  factor in combination with a low impedance level. For example, at 10 MHz, a macroscopic quartz resonator typically exhibits a  $Q \sim 100\,000$  and  $R_m \sim 50\,\Omega$ . Capacitive MEMS resonators exhibit similar  $Q$ -factor as quartz, but have a higher impedance at resonance, as is evident from table 6, and thus a lower  $FOM_{1,2}$  at fixed oscillation frequency. Piezoelectric MEMS oscillators show an inferior  $FOM_{1,2}$  compared to capacitive MEMS oscillators running at the same frequency. This seems counterintuitive at first glance, since piezoelectric MEMS resonators exhibit lower impedance compared to capacitive MEMS resonators. However, this behavior can be explained by the fact that piezoelectric MEMS resonators show a lower  $Q$  compared to capacitive MEMS and quartz. From tables 5 and 6, it is also observed that the maximum frequency for a piezoelectric oscillator is  $\sim 1$  GHz while the highest frequency achieved with a capacitive oscillator is only  $\sim 100$  MHz. This is explained by the fact that at higher frequencies the impedance of a piezoelectric resonator tends to decrease and is capable to keep up with the parallel impedance of the shunt capacitor  $C_s$ . Therefore, the oscillation condition described by (17) is maintained irrespective of the oscillation frequency. In contrast, the impedance of capacitive MEMS resonators is relatively insensitive to frequency scaling since it is determined by the gap width  $g$  which is typically not scaled down with the other resonator dimensions that set the resonance frequency, as is visible in figure 12. Finally, it can be seen that both the  $FOM_1 \sim -100$  and  $FOM_2 \sim -90$  for an LC oscillator are inferior to most capacitive and piezoelectric MEMS oscillators underpinning the advantage of MEMS-based oscillators compared to CMOS-based oscillator. The best FOMs reported for both the capacitive and piezoelectric MEMS oscillators are similar to the FOMs typically reported for quartz and lie in the  $-135$  to  $-140$  range for  $FOM_1$  and between  $-125$  and  $-130$  for  $FOM_2$ .

In figure 19, the noise is plotted at an off-set frequency far away from the carrier, i.e. where the spectrum has flattened

**Table 5.** Overview of literature data on piezoelectric transduced oscillator's resonance frequency, near carrier roll-off, near carrier noise, noise floor, oscillator power consumption, resonator  $Q$ -factor, resonance mode and resonator's motional impedance. Data are sorted to FOM<sub>1</sub>.

Reference	Center frequency (MHz)	Near carrier roll-off	Noise at 1 kHz (dBc Hz <sup>-1</sup> )	FOM <sub>1</sub> (dBc Hz <sup>-1</sup> )	FOM <sub>2</sub> (dBc Hz <sup>-1</sup> ) mW <sup>-1</sup>	Noise floor (dBc Hz <sup>-1</sup> )	Power consumption (mW)	$Q$ -factor	Mode	$R_m$ ( $\Omega$ )
[112]	600	$1/f^3, 1/f^2$	-100	-136	-128	-150	5.6	2000	AlN bulk	
[113]	1006	$1/f^3$	-95	-135	-126	-150	7.2	7100	AlN on Si bulk	1.5E+02
[200]	1500	$1/f^3, 1/f^2$	-86	-130	-130	-150	1		AlN bulk	
[111]	496	$1/f^3$	-92	-126	-116	-147	9.4	3800	AlN on Si bulk	6.0E+02
[107]	1050	$1/f^3$	-81	-121	-116	-146	3.5		AlN bulk	
[73]	2000	$1/f^2$	-75	-121	-115	-140	4	700	AlN bulk	3.0E+01
[108]	208	$1/f^3$	-94	-120		-152		6100	AlN on Si bulk	7.0E+01
[53]	223	$1/f^3$	-88	-115	-105	-160	10	2100	AlN bulk	3.5E+01
[106]	222	$1/f^3$	-88	-115	-105	-160	10	2100	AlN bulk	3.5E+01
[109]	427	$1/f^3$	-82	-115	-103	-147	13	1400	AlN on Si bulk	1.8E+02
[106]	307		-84	-114	-104	-151	10	1400	AlN bulk	2.6E+01
[110]	467	$1/f^3$	-80	-113	-104	-145	9.4	1850	ZnO+c- C+SiO <sub>2</sub>	6.0E+02
[75]	101.7	$1/f^3$	-90.6	-111	-99		15.6	1257	AlN bulk	1.1E+03
[77]	106	$1/f^3, 1/f^2$	-88	-108	-113	-145	0.34	4000	AlN on Si bulk	2.5E+02
[106]	176		-79	-104	-94	-153	10	1500	AlN bulk	7.1E+01
[106]	482		-68	-102	-92	-145	10	850	AlN bulk	9.2E+01
[75]	78.8	$1/f^3$	-80.8	-99	-88		11.8	1061	AlN bulk	7.9E+02
[75]	19.56	$1/f^3$	-79.8	-86	-82		2.5	786	AlN bulk	8.1E+03
[105]	1		-100	-80	-105	-110	3.0E-03	140 000	AlN on Si bulk	2.0E+02

**Table 6.** Overview of literature data on capacitive transduced oscillator's resonance frequency, near carrier roll-off, near carrier noise, noise floor, oscillator power consumption, resonator  $Q$ -factor, resonance mode, resonator's motional impedance, resonator bias and transducer gap width. Data are sorted to FOM<sub>1</sub>.

Reference	Center frequency (MHz)	Near carrier roll-off	noise at 1 kHz (dBc Hz <sup>-1</sup> )	FOM <sub>1</sub> (dBc Hz <sup>-1</sup> )	FOM <sub>2</sub> (dBc Hz <sup>-1</sup> ) mW <sup>-1</sup>	Noise floor (dBc Hz <sup>-1</sup> )	Power consumption (mW)	$Q$ -factor	Mode	$R_m$ ( $\Omega$ )	Bias voltage (V)	Gap (nm)
[124]	13.1	$1/f^3$	-138	-140		-149		130 000	Si bulk	4.5E+03	100	750
[131]	145.0	$1/f^3$	-111	-134	-129	-133	3.6	51 000	Si bulk	2.4E+03	14	77
[130]	103.0	$1/f^2$	-108	-128	-124	-136	2.6	80 000	Si bulk	5.0E+03	18	200
[123]	13.0	$1/f^3$	-120	-122	-128	-147	0.24	100 000	Si bulk	5.0E+02	20	180
[122]	12.0	$1/f^3$	-115	-117		-120		180 000	Si bulk	1.5E+06	100	1000
[128]	61.2	$1/f^3$	-100	-116	-116	-130	0.95	48 000	Si bulk	1.5E+03	12	80
[67]	61.0	$1/f^2$	-100	-116		-110		130 000	Si bulk	2.6E+03	16	92
[66]	15.4	$1/f^3, 1/f^2$	-109	-113		-133		4360	Si flex	2.2E+04	30	300
[67]	59.9	$1/f^3$	-95	-111		-125		6200	Si bulk	9.7E+02	16	32
[126]	14.0	$1/f^3$	-105	-108		-120		1500	Si flex	1.0E+06	130	1000
[118]	5.1	$1/f^3$	-105	-99				80 000	Si flex	3.5E+04	5	400
[62]	10.0	$1/f^2$	-95	-95	-96	-110	0.82	1036	Si flex	3.4E+02	13	100
[62]	10.0	$1/f^3$	-80	-80	-81	-120	0.82	1036	Si flex	3.4E+02	13	100
[121]	9.8	$1/f^3$	-80	-80		-120		3600	Si flex	1.8E+04	7	100
[114]	0.02					-70		51 000	Si flex	2.5E+06	32	2000
[116]	1.0					-88			Si flex		7	
[104]	2.2					-90		1160 000	Si bulk	7.6E+04	60	3000



out and the noise floor is reached. It can be seen that the noise floor reported for most piezoelectric oscillators is approximately  $-150 \text{ dBc Hz}^{-1}$ , which is slightly better than the  $-140$  to  $-145 \text{ dBc Hz}^{-1}$  typically reported for quartz. These values are most likely not limited by the resonator itself, but by the signal-to-noise ratio (SNR) at the input of the buffer amplifier that feeds the signal to the outside world. This SNR is improved when going to higher frequencies, since delivered power increases with frequency for a fixed voltage swing while the (white) noise contribution stays constant. This scaling behavior might explain the lower noise floor for the high frequency piezoelectric MEMS resonator compared to the quartz oscillator running at a lower frequency. In contrast, it can be seen that the noise floor of most capacitive MEMS oscillators is considerably higher than what is achieved for quartz, even at high frequencies. This might be explained by the high impedance level  $R_m$  at resonance and the associated attenuation of the signal through the resonator. This leads to low power levels  $P_0$  at the amplifier input and hence a small SNR.

Overall, it can be concluded that the noise performance of MEMS close to the carrier frequency as is captured by  $\text{FOM}_1$  and  $\text{FOM}_2$  can be, in best cases, as good as the FOMs reported for a typical quartz oscillator and is much better than the values reported for LC based or any other type of electrical oscillator. Although the FOMs for capacitive and piezoelectric MEMS are similar, the reason for this is quite different. Low FOMs for capacitive MEMS are most likely directly related to the high  $Q$ -factor that can be obtained with this type of resonator. The low FOM is in this case achieved in spite of the relatively large impedance that is associated with a capacitive resonator. The low FOMs that are achievable with piezoelectric MEMS are most likely a direct result of their low impedance, even in spite of the relatively low  $Q$  that is achieved with piezoelectric MEMS. The noise floor of piezoelectric MEMS oscillators tends to be slightly lower than for quartz and is most likely a result of the higher oscillation frequency that can be achieved with piezoelectric MEMS. The noise floor of capacitive MEMS oscillators tends to be higher than quartz, even at higher oscillation frequencies. This can be explained by the high impedance of capacitive MEMS and associated small signal levels and therefore low SNR at the resonator output.

#### 4.5. Active transduction schemes

Capacitive resonators have the intrinsic disadvantage of having relatively high impedance compared to piezoelectric transduced resonators, as is explained in the previous sections. These limitations find their origin in the small coupling factor that can be achieved with capacitive transduction, especially at high resonance frequencies. The coupling factor can be increased by reducing the transduction gap, but apart from the limitations set by the processing this also leads to nonlinear behavior of the coupling factor for large resonator displacements and to up-conversion of flicker noise in the oscillator loop as a result. However, an advantage of capacitive transduction is that it allows for the use of

single crystal silicon (SCS) as the resonating medium without the need of having lossy metal electrodes present at its surface, as is the case in piezoelectric resonators. For this reason, silicon resonators typically show a higher  $Q$  and very little aging, as is explained in sections 4.2 and 5.1. Furthermore, SCS resonators are relatively easy to process and packaged on wafer level as is explained in section 2. Therefore, several alternatives are investigated that increase the coupling factor of silicon resonators without having to resort to the more lossy piezoelectric media and metal electrodes. These alternative transduction schemes consume dc power and are therefore called ‘active’ transduction schemes. Active transduction schemes are capable of generating signal amplification and the output current per unit of resonator displacement can be many times larger compared to capacitive resonators. Therefore, these resonators exhibit considerably lower effective impedance compared to their capacitive counterparts. In some cases the effective impedance can even be made zero or negative, i.e. the resonator itself functions as an amplifier. Furthermore, large resonator displacements are not necessarily required to deliver sufficient output power  $P_0$ , since much larger output currents can be generated per unit of resonator displacement. Small resonator displacements lead to small variations of the transduction gap and therefore suppress transduction nonlinearities and up conversion of flicker noise in the oscillator loop as a result.

The first reported MEMS resonator based on active transduction constituted a resonating gate transistor [50, 168]. The freestanding gate cantilever is brought into mechanical resonance and modulates the gate capacitance, see figure 20. The cantilever is biased with a dc voltage. As a result, the electric field between in-gate and the source–drain channel is varied resulting in a modulation of the channel resistance. In this case, the resonating element is a surface micro-machined metallic beam and therefore still exhibits a relatively low  $Q$  of only 67 at 30 kHz. However, a similar principle is also demonstrated using a SCS resonator [169–171] resulting in a measured  $Q = 7000$  at 2.4 MHz. In this case, a resonating source–drain channel instead of a resonating gate is used, as is depicted in figure 21. It has been shown that these structures can provide more than unity gain and thus an effective *negative* impedance thereby allowing for autonomous oscillation without the use of an external sustaining amplifier [169, 172]. In [169], also a 70 MHz resonator with a  $Q$ -factor of 15 400 is demonstrated based on the same principle. In this case, an effective impedance of 55 k $\Omega$  is achieved, which is a fivefold reduction compared to the motional impedance caused by the capacitive transduction. The relative ineffectiveness of the FET transduction at higher frequencies can be explained by the fact that the transduction efficiency depends directly on field modulation in the gap which is largest for large resonator excursions. Large resonator excursions can be achieved when the spring constant and hence resonance frequency of the resonator is made low. The level of field modulation can also be increased when the gap is made narrow. However, resonators with a small transduction gap have a tendency to behave nonlinearly, similar to electrostatic resonators, and therefore limited power handling and more upconversion of flicker noise can be expected as a result.

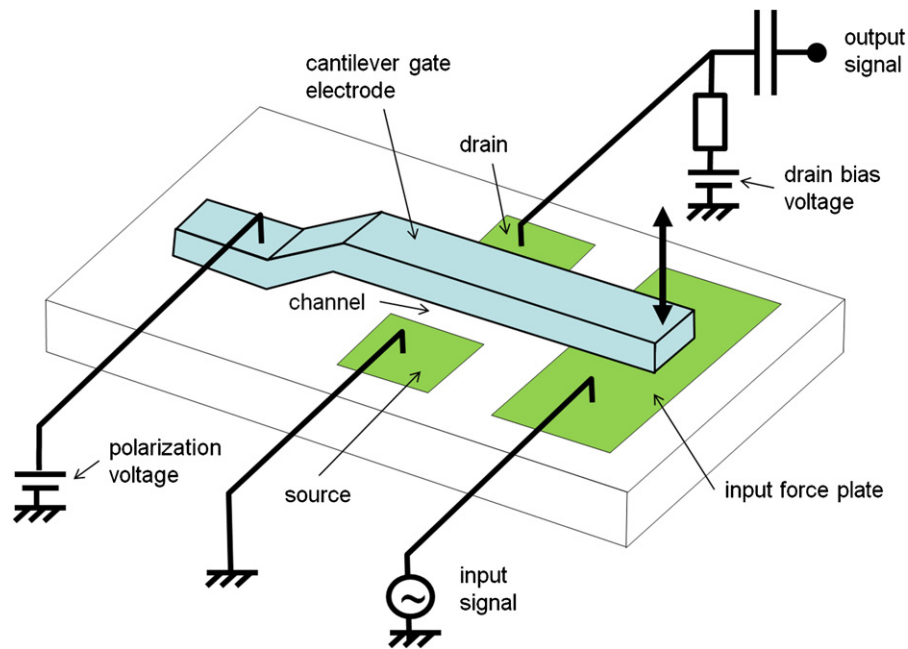


**Figure 20.** Schematic layout of a resonating gate FET. The freestanding gate cantilever is brought into mechanical resonance and modulates the gate capacitance and the resistance in the source–drain channel.

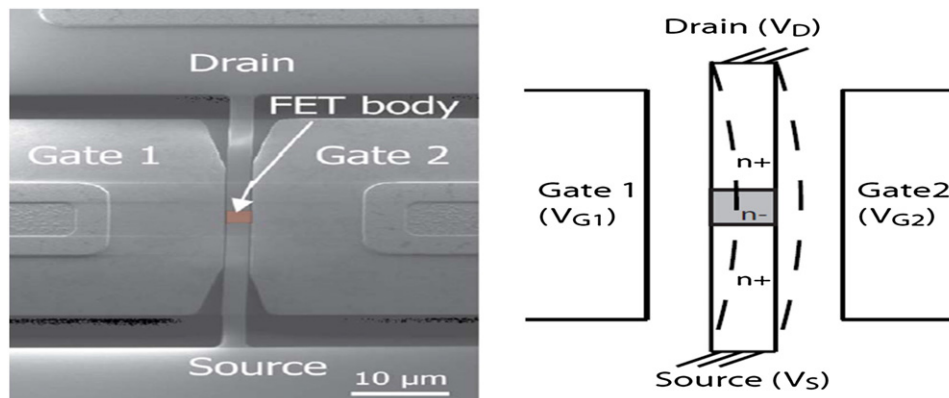


**Figure 21.** SEM image and schematic layout of a vibrating body FET. An ac voltage is applied on gates 1 and 2 bringing the source–drain channel into resonance. The motion of the resonator causes a modulation of the electric field in the gap, which induces a field effect in the source–drain channel.

Instead of detecting gap modulation, as is done in capacitive and FET-based resonators, also a direct measurement of mechanical strain that is build up inside the resonator can be used to sense its motion [173], as is depicted in figure 22. The mechanical strain is detected by means of the piezoresistive effect. Although silicon is not piezoelectric, it exhibits a strong piezoresistive effect and therefore resonators made from Si, and SCS in specific, are well suited to adapt this transduction principle. In this way, strain rather than gap variation is the parameter that is being sensed and therefore nonlinearities associated with capacitive sensing as is described in section 4.1 can be suppressed without sacrificing the magnitude of the resonator's output current  $i$ . The output current can be tailored by the dc bias current that is sent through the resonator. In [173], a piezoresistive 10 MHz resonator is demonstrated with a very high  $Q$ -factor of 125 000. The piezoresistive readout shows a 130-fold reduction in

effective impedance compared to capacitive readout. It has also been shown that piezoresistive resonators can exhibit above-unity gain, and therefore an effective *negative* motional impedance at 15 MHz with  $Q = 60\,000$  [174]. Furthermore, because the transduction efficiency does not depend directly on the resonator stiffness, it is demonstrated that the output signal is insensitive to geometric scaling and is therefore suitable for achieving high resonance frequencies. Fundamental mode resonators with resonance frequency at 1.1 GHz with  $Q = 550$  [175] and higher order modes up to 4.5 GHz with  $Q = 11\,200$  [86] and more recently even upto 40 GHz with  $Q = 130$  [176] have been demonstrated. It is shown that at 1.1 GHz, the effective impedance is reduced by orders of magnitude as a result of the piezoresistive instead of capacitive readout. Also thermal actuation can be used in combination with piezoresistive sensing to form resonators and oscillators [177–182]. A beneficial feature of thermal rather than

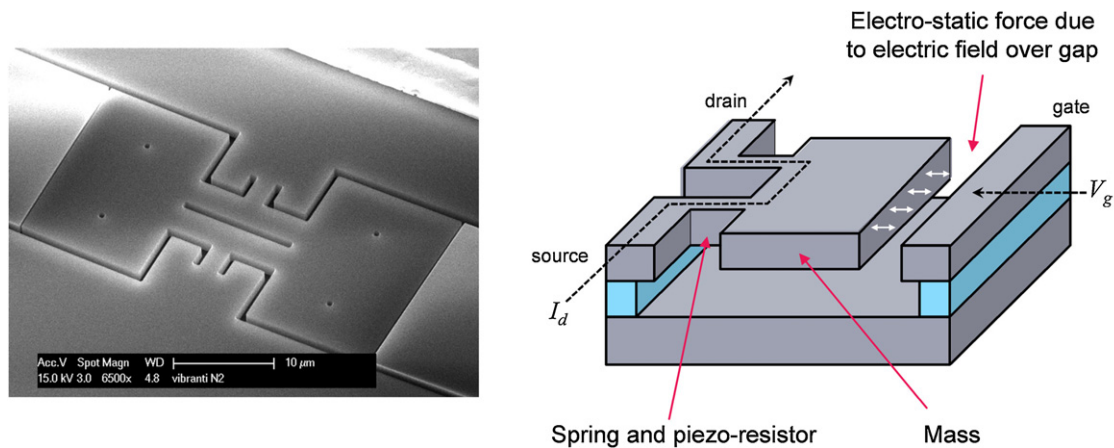


**Figure 22.** SEM image and schematic layout of a piezoresistive resonator. An ac voltage is applied to the gate bringing the resonator into resonance. The resonance causes a variation in mechanical strain inside the resonating body, which is sensed using the piezoresistive effect in silicon.

capacitive actuation is that in this case the feed through capacitance  $C_s$  is not linked to the actuation force and can be minimized without affecting the coupling factor.

One important characteristic of the above-mentioned active transduction schemes is that in addition to mechanical noise, now the resonator is also a source of electrical noise (white noise, flicker noise, shot noise) originating from the electrical energy dissipation in the source–drain channel when the field effect is used or in the resistor when the piezoresistive effect is used. Obviously, these additional noise sources need to be taken into account when optimizing the phase noise of the oscillator. Nevertheless, it is demonstrated that oscillators based on piezoresistive transduction are capable of exhibiting a low  $FOM_1 = -117$  and  $FOM_2 = -109$  [183].

## 5. Deterministic frequency stability and accuracy

Apart from noise requirements or non-deterministic frequency stability, an oscillator has to fulfill requirements regarding its deterministic frequency stability and absolute accuracy. For many applications, the specification for frequency accuracy is less than a few hundred parts per million (ppm) down to a few ppm. The accuracy of the oscillator is almost completely determined by the resonator itself, since it typically exhibits a large  $Q$ , see also equation (18). The accuracy of the resonator, and thus the oscillator, is determined by the resonator's temperature drift, aging behavior and manufacturing accuracy.

### 5.1. Resonator stability, temperature drift and aging

The stability of a reference oscillator during its operational lifetime can be deteriorated as a result of changes in the ambient environment, such as temperature fluctuations, bias fluctuations and material wear. The overall fluctuations of all these factors should stay typically well below 100 ppm for many applications. The variation of the frequency with temperature is an important factor determining the overall frequency stability of the resonator. Quartz resonators have excellent temperature stability since the linear and in some cases even the quadratic component of the temperature

dependence can be canceled by choosing the optimum resonance mode in combination with an optimum crystal orientation leaving at best a residual dependence of about 1 ppm over a temperature window of 100 °C [51]. In contrast, the uncompensated temperature stability of Si- and AlN-based MEMS resonators is approximately  $-30$  ppm/°C, which is equivalent to 3000 ppm over 100 °C, and can be attributed to the relatively large negative first order temperature coefficient (TC) of Young's modulus of Si and AlN. However, several approaches exist for the compensation of the temperature drift. These approaches can be divided into five categories ranging from resonator level solutions to oscillator level concepts, as is schematically depicted in figure 23. Most often, the different approaches can be combined to further improve temperature stability.

By stabilizing the temperature of the resonator, the temperature drift of the oscillator frequency is minimized. Although proven to be very effective, this technique suffers from large power consumption. However, the small resonator size allows for a better power efficiency than what can be achieved with oven-controlled quartz oscillators. In [184], the ambient temperature is sensed using a PTAT sensor that drives a dc current through the resonator. The dc current results in Joule heating and temperature control of the resonator. A more direct and precise way of sensing the resonator temperature is based on the difference in TC of two resonance modes [185] or two separated resonators with different TCs [186]. A very high degree of frequency stability is achieved of only 0.1 ppm over 100 K by stabilizing the frequency difference of the two resonators with different TCs [186].

The compensation of the temperature dependence of Young's modulus can be achieved through material modification of the resonator. Silicon, AlN and most other materials exhibit a negative temperature dependence of Young's modulus. When these materials are combined with a material with an opposite signed Young's modulus, such as SiO<sub>2</sub>, then temperature drift compensation is achieved [187–192]. Figure 24 shows the temperature drift of an oxidized Si resonator compared to an un-oxidized resonator, AT-cut quartz resonator and a tuning fork quartz resonator.

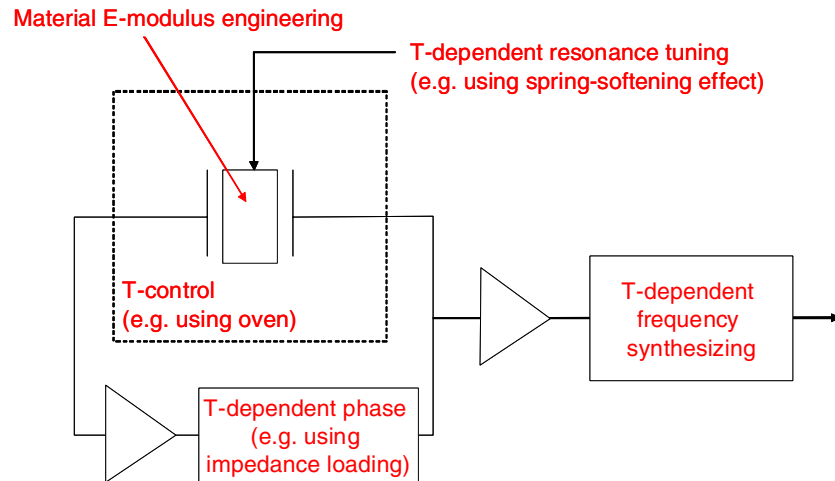


**Figure 23.** Five approaches exist for the compensation of the temperature-induced frequency drift of a MEMS resonator ranging from resonator level solutions to oscillator level concepts.

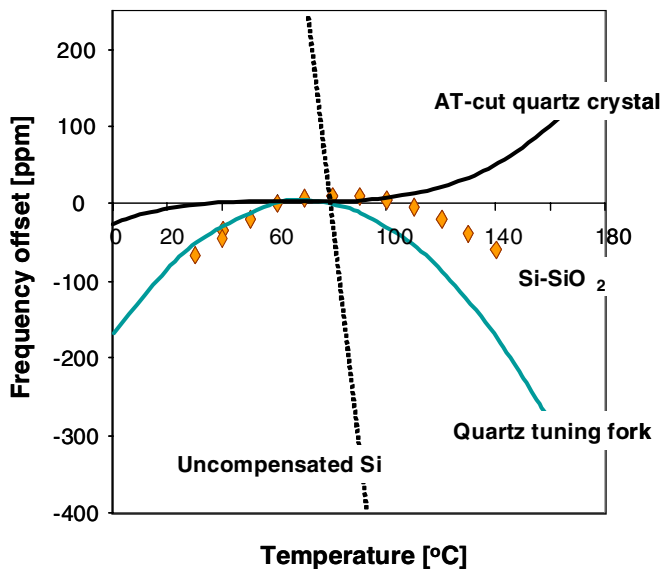


**Figure 24.** Frequency shift as a function of frequency for AT-cut quartz, tuning fork quartz, Si and oxidized silicon resonator.

It can be seen that the first order temperature drift can be fully compensated for by the thermal oxidation. However, higher order drift terms remain and can be attributed to higher order drift terms of the SCS itself. Furthermore, the oxidation causes a considerable shift of frequency at fixed temperature, which poses limits to overall accuracy [193]. Charging of the oxide has been observed, which causes spring softening of the resonator and can detune the resonance frequency as a result [194]. Therefore, the charging effect might also have consequences for the aging behavior of the resonator when a bias voltage is applied to the resonator over prolonged periods of time [195]. An alternative approach is to modify the temperature dependence of the Si Young's modulus itself. This is achieved by heavily doping [182, 196, 197] or depleting the silicon [198, 199]. In this way, the frequency drift of a MEMS resonator can be lowered down to  $-1.5 \text{ ppm K}^{-1}$ .

Impedance loading can be used to slightly detune the loop phase and as a result the oscillation frequency [200, 201],

as was explained in section 3.2. For example, adding more shunt capacitance  $C_s$  will shift the loop phase thereby slightly shifting the oscillation frequency. However, when the phase shift is made too large, the oscillator will start oscillating at a frequency outside the capture window of the resonator and the large phase selectivity of the resonator cannot be used and hence  $Q_{\text{loaded}}$  will be very low. Therefore, impedance loading can only be used to offset relatively small changes in frequency in the order of  $1/Q$ , which is often not sufficient to compensate the full temperature window and should be combined with other methods.

Tuning of the mechanical resonance frequency can be used for temperature stabilizing the oscillator when the tuning parameter can be made temperature dependent in such a way that it offsets the temperature drift of Young's modulus. An important tuning mechanism is based on the spring softening effect as described by the first term of the Taylor expansion in (44):

$$F_{\text{softening}} = -V_{dc}^2 \frac{\epsilon_0 A}{g^3} x. \quad (45)$$

This term describes an electrostatic force that is proportional to the resonator displacement  $x$  as a result of an increase in the field strength caused by a changing gap width. It can therefore be considered as a spring with a bias voltage-dependent negative spring constant. This negative spring constant is subtracted from the mechanical spring constant to give the total spring constant of the resonator. Making the bias voltage a function of temperature allows for the compensation of temperature drift of the mechanical spring constant of the resonator. An alternative approach that uses the same physical effect is to make the gap width a function of temperature which can be accomplished through thermal expansion mismatch [202]. In both cases, only capacitive resonators with relatively low mechanical spring constant, and thus a low resonance frequency, can be compensated over the full temperature window. The spring softening effect is too small to compensate for large changes in the spring constant that occur in high frequency, high stiffness resonators without having to resort to very narrow gaps or high bias voltages. Spring softening



**Table 7.** Comparison of temperature drift compensation techniques.

Method	Frequency shift (ppm)	Temperature window (K)	Average drift over $T$ window (ppm K <sup>-1</sup> )	Reference
Spring softening	380	90	4.2	[203]
E modulus engineering, SiO <sub>2</sub> + ZnO + Si	244	60	4.1	[188]
E modulus engineering, Si depletion	216	60	3.6	[198]
E modulus engineering, Si depletion	180	60	3.0	[199]
Spring softening	237	90	2.6	[205]
E modulus engineering, degenerate doping of Si	88	60	1.5	[196]
E modulus engineering, SiO <sub>2</sub> + AlN	300	225	1.3	[187]
E modulus engineering, SiO <sub>2</sub> + Si	180	160	1.1	[190]
E modulus engineering, SiO <sub>2</sub> + Si	100	110	0.9	[193]
Frequency synthesizer	100	125	0.8	[218]
E modulus engineering, degenerate doping of Si			0.4	[182]
Oven control	39	100	0.4	[184]
Spring softening	39	100	0.4	[204]
Frequency synthesizer	20	70	0.3	[219]
Spring softening	19	80	0.2	[202]
Impedance loading + E modulus engineering	20	100	0.2	[200]
Frequency synthesizer	9	50	0.2	[206]
Frequency synthesizer + resonator tuning	2	130	0.02	[163, 209]
Oven control + E modulus engineering	0.1	100	0.001	[186]

techniques have been demonstrated for oscillation frequencies upto 6 MHz [203–205]. It should furthermore be realized that the spring softening effect is only present for capacitive parallel plate transduction and is absent in interdigital comb drives and piezoelectric transduced resonators. A drawback of these tuning concepts is that the parameter to be tuned should only be temperature dependent, and not be dependent on other variables such as supply voltage and package stress that might not be controlled at sufficiently high levels.

The oscillator level approach that is capable of TC compensation is based on frequency synthesizer techniques. The output frequency of the oscillator is altered using a frequency divider or multiplier connected to the oscillator output. By adjusting the division or multiplication ratio with temperature, it is possible to offset the TC of the oscillator frequency and create a stable frequency at the output of the divider or multiplier. In this manner, not only compensation of the TC is achieved, but the same technique is also capable of offsetting frequency errors caused by fabrication tolerance and it renders obsolete the one frequency one crystal unit paradigm since a single resonator can be used for the generation of many frequencies over a large frequency band [206]. Obviously, the frequency synthesizer technique can also be used for the TC compensation of quartz and electrical oscillators and is not unique to MEMS. For an LC oscillator frequency stability down to 100 ppm over a temperature window of 70 K has been demonstrated [207, 208]. For capacitive MEMS, the stability can be as low as 20 ppm over 70 K for commercially available oscillators using this technique. The higher degree of stability obtained for MEMS can probably be explained by the higher  $Q$  factor of the resonator. A MEMS oscillator is therefore less sensitive to external factors that affect the overall drift of the oscillator, other than the well-defined TC of the resonator itself.

Table 7 gives an overview what is achieved for the different concepts by various groups. Concepts based on E-modulus material engineering show relatively poor

performance. This is caused either by higher order drift of the TC when an oxide layer is used [187, 188, 190, 193, 196] or by an incomplete cancellation of the first order term when very high doping levels or fully depleted silicon is used [198, 199]. However, E-modulus engineering can easily be combined with other techniques to further improve the stability. The use of a Si-SiO<sub>2</sub> capacitive resonator in combination with oven control has been shown to result in very good temperature stability of only 0.1 ppm [186]. In [200], a stability of 20 ppm is obtained over a large temperature window of 100 K using a 1.5 GHz AlN-SiO<sub>2</sub> FBAR resonator in combination with temperature-dependent impedance loading. In [163, 209], a frequency synthesizer technique is demonstrated in combination with frequency tuning of the resonator resulting in a very good frequency stability of only 2 ppm over a wide temperature range of 130 K.

Another source for resonator instability is caused by aging of the resonator itself. For this reason, aging of quartz resonators has been studied extensively and is e.g. reviewed in [210–213]. For SCS electrostatic resonators, it has been shown that the level of aging is very much dependent on the resonator ambient and instabilities that are caused by absorption and desorption of molecules at the resonator surface [12, 214]. Resonators measured in an open ambient showed more than 10 ppm of frequency variation over 1000 h, while resonators sealed in a package showed only a few ppm of shift. When the resonator is sealed from the environment using proper packaging techniques in combination with a high temperature anneal it has been demonstrated that the stability of resonant frequency for both long-term operation of more than a year and large number of temperature cycles is within a few ppm [16, 39], thereby rivaling or even exceeding the aging characteristics of quartz [40]. For AlN-based piezoelectric resonators, very little or no aging data are available in the open literature [215]. Mechanical acceleration is also known to have an effect on the deterministic frequency stability of



quartz oscillators [216, 217]. In [63], this effect is studied for a capacitive MEMS oscillator.

### 5.2. Manufacturing accuracy and trimming

Reference oscillators have to meet not only strict stability criteria, as has been discussed in the previous section, but often their absolute frequency needs to be within a predefined window as well. Variations of the resonator's eigenfrequency can occur as a result of variations in their manufacturing process. Geometry variations as a result of layer thickness, lithographic or etch variations result in variations in the order of 1000 ppm in the resonance frequency of the resonator [220]. Most applications require frequency accuracy well below 100 ppm and therefore this process-induced variation needs to be accounted for. Several approaches have been demonstrated for suppressing process-induced variations in resonance frequency and are reviewed in [221].

For a quartz resonator, process-induced frequency variations are trimmed using a mass loading technique. Material is added to the resonator using physical vapor deposition (PVD). As a result, the resonator mass or stiffness is changed and a shift in frequency occurs. The change in frequency is monitored during the trimming process and tuned to fix the frequency within ppm level accuracy. Although a viable and widely used technique to trim quartz, mass loading is very difficult to implement for MEMS resonators. MEMS resonators are relatively sensitive to unintended mass loading due to their much smaller size compared to a typical quartz crystal. Therefore, the MEMS resonator after trimming should be kept under well-defined ambient conditions. In practice, this implies that the MEMS resonator should be trimmed after it has been sealed from ambient environment, i.e. when it is already packaged using the techniques described in section 2. Obviously, this means that the PVD trimming technique used in quartz industry cannot be used and sets strict limitations to other trimming technique being applied. However, several techniques have been reported that allow for permanently changing the resonator's frequency after it has been packaged. In [222] it is shown that Joule heating of a Si electrostatic resonator can lead to a permanent change in frequency and can be used for reaching a predefined value. Also a laser ablation technique of a packaged resonator has been proposed for trimming its frequency [223]. In this case, a transparent package is used to give the laser access to the resonator cavity.

Several other methods have been reported that avoid the use of frequency trimming. By careful design of the resonator it is possible to make the resonance frequency depend only very little on certain geometric variations. For example, lateral variations in the resonator geometry do not have to result in a shift of resonance frequency when the resonator mass is varied by the same amount as the resonator stiffness, as can be understood from (8). In this case, the resonance frequency is not affected by geometric variation since the frequency only depends on the ratio of resonator mass and stiffness. Using this approach, the frequency variation can be reduced to a few hundred ppm [224–226]. Another approach is based on resonator redundancy [227]. In this case, an array of

similar resonators is linked to a unique oscillator. Switching from one resonator to the other is performed when the frequency of the resonator in use is out of range. In principle, this technique can also be used to compensate for temperature drift. None of the techniques described above have been capable of ppm level frequency accuracy that is required for most applications. A technique that is capable of achieving the required ppm level accuracy is based on frequency synthesis and is very similar to the frequency synthesis technique used to offset the temperature drift of the resonator, as is explained in section 5.1. In this case, the frequency of the resonator is not altered but the output frequency of the oscillator is modified instead. The output frequency of the oscillator is modified by dividing or multiplying the original frequency in such a way that a predefined frequency is reached [206].

## 6. Conclusion

MEMS-based oscillators allow for higher levels of system integration at low cost, compared to established quartz technology. These advantages are a direct result of the material compatibility with standard CMOS production and the batch type of processing of both the resonator and its package. In particular, surface micro-machined on-wafer thin film packages result in a very small form factor, low cost package that is in many cases compatible with existing CMOS infrastructure. The resonator can in principle be processed and sealed on the same chip that holds the CMOS circuitry that is required to drive the resonator into oscillation, but the MEMS can also be processed on a separate die and integrated with the CMOS die inside the same standard low cost plastic package.

A good MEMS oscillator needs to have a stable long-term as well as short-term output frequency. Short-term frequency fluctuations translate into phase noise and find their cause in the presence of non-deterministic noise sources, such as white and flicker noise. It is shown that the resonator should have low impedance, high  $Q$ -factor and good power handling in order to suppress the effects of these noise sources on the overall phase noise of the oscillator. Capacitive, piezoelectric and active transduced resonators are compared. Capacitive, silicon-based resonators can offer very high  $Q$ -factors approaching the values obtained with quartz when they are sealed in a package that is capable to maintain a gas pressure well below one atmosphere in order to eliminate the effects of gas damping on the resonator  $Q$ -factor. However, capacitive Si resonators suffer from high impedance due to the relatively low electro-mechanical coupling that is associated with capacitive transduction. The piezoelectric effect allows for much larger electro-mechanical coupling factors and hence piezoelectric transduced resonators exhibit much lower impedance. However, the  $Q$ -factor of AlN-based piezoelectric resonators tend to be lower for a given frequency than their Si-based counterparts. Most piezoelectric as well as capacitive transduced oscillators demonstrated so far show a FOM that is superior to the FOM of LC-based oscillators and in best cases comparable to the FOM that is obtained for a typical quartz oscillator. An alternative to the trade-off between low resonator impedance and high  $Q$ -factor, as is characteristic for

piezoelectric and capacitive transduced resonators, is active transduced resonators. With active transduced resonators, it is possible to achieve high  $Q$ -factors since they are made of SCS. They are also capable of generating large output currents at resonance by exploiting the field effect and piezoresistive effect in Si. Therefore, their effective impedance can be made much lower compared to capacitive transduced resonators and in some cases the impedance can even be made negative, i.e. the active transduced resonator is capable of signal amplification. The large output current combined with the high  $Q$ -factor that is typical for Si can result in a good phase noise performance as has been demonstrated for a piezoresistive oscillator.

The long-term frequency stability of a MEMS oscillator is mainly determined by the temperature drift and aging characteristics of the resonator. The temperature dependence of AlN as well as Si Young's modulus causes a shift in resonance frequency over ambient temperature of a few thousand ppm which is much larger than the <100 ppm that is typically observed in a quartz resonator. Several methods are described to suppress this temperature drift and to achieve frequency stability in the sub-ppm range in best cases. These methods range from resonator level compensation, e.g. through material engineering or temperature-dependent bias tuning, to oscillator level compensation, e.g. using temperature-dependent impedance loading or frequency synthesis. For Si-based resonators, it is demonstrated that aging of the resonance frequency can be less than a few ppm and is strongly dependent on the hermeticity of the resonator package.

It is concluded that MEMS-based oscillators fill the application gap between high-performance non-CMOS compatible quartz technology on the one hand, and low-performance CMOS compatible LC oscillators on the other hand. The electrical performance of the best MEMS oscillators reported to date rivals the performance of typical quartz oscillators while allowing for higher levels of system and package integration than what is possible with present day quartz technology.

## References

- [1] Frerking M E 1996 Fifty years of progress in quartz crystal frequency standards *Proc. IEEE Int. Freq. Control. Symp.* pp 33–46
- [2] Fujishima S 2000 The history of ceramic filters *IEEE Trans. Ultrason. Ferroelectr. Freq. Control* **47** 1–7
- [3] Lacaita A, Levantino S and Samori C 2007 *Integrated Frequency Synthesizers for Wireless Systems* (Cambridge: Cambridge University Press)
- [4] Nguyen C T 2007 MEMS technology for timing and frequency control *IEEE Trans. UFFC* **33** 251–70
- [5] Lam C S 2008 A review of the recent development of MEMS and crystal oscillators and their impacts on the frequency control products industry *IEEE Ultrasonics Symp.* pp 694–704
- [6] Hsu W T 2008 Recent progress in silicon MEMS oscillators *Proc. 40th Annual Precise Time and Time Interval (PTTI) Meeting* pp 135–46
- [7] Tabatabaei S and Partridge A 2010 Silicon MEMS oscillators for high-speed digital systems *IEEE Micro* **30** 80–9
- [8] Enz C C, Baborowski J, Chabloz J, Kucera M, Muller C, Ruffieux D and Scolari N 2007 Ultra low-power MEMS-based radio for wireless sensor networks *18th European Conf. on Circuit Theory and Design (ECCTD)* pp 320–31
- [9] Senturia S D 2002 *Microsystem Design* (Dordrecht: Kluwer)
- [10] Hsu W T 2007 Low cost packages for MEMS oscillators *Int. Electronics Manufacturing Technology Symp.* pp 273–7
- [11] Pelzer R, Kirchberger H and Kettner P 2005 Wafer-to-wafer bonding techniques: from MEMS packaging to IC integration applications *6th Int. Conf. on Electronic Packaging Technology* pp 1–6
- [12] Kaajakari V, Kiihamaki J, Oja A, Seppo H, Pietikainen S, Kokkala V and Kuisma H 2005 Stability of wafer level vacuum encapsulated single-crystal silicon resonators *Proc. Transducers* pp 916–9
- [13] Lin C H, Lu J M and Fang W 2005 Encapsulation of film bulk acoustic resonator filters using a wafer-level microcap array *J. Micromech. Microeng.* **15** 1433–8
- [14] Theunis F, Lisec T, Reinert W, Bielen J, Yang D, de Jongh M and Krusemann P V E 2007 A novel and efficient packaging technology for RF-MEMS devices *Proc. 57th Electronic Components and Technology Conf., ECTC'07* pp 1239–45
- [15] Cheng Y T, Lin L and Najafi K 2000 Fabrication and hermeticity testing of a glass-silicon package formed using localized aluminum/silicon-to-glass bonding *13th Annual Int. Conf. on Micro Electro Mechanical Systems (MEMS)* pp 757–62
- [16] Hsu W T 2006 Reliability of silicon resonator oscillators *IEEE Int. Frequency Control Symp. and Exposition* pp 389–92
- [17] Legtenberg R and Tilmans H A C 1994 Electrostatically driven vacuum-encapsulated polysilicon resonators. Part I: design and fabrication *Sensors Actuators A* **45** 57–66
- [18] Legtenberg R and Tilmans H A C 1994 Electrostatically driven vacuum-encapsulated polysilicon resonators. Part I: theory and performance *Sensors Actuators A* **45** 67–84
- [19] Hochst A *et al* 2004 Stable thin film encapsulation of acceleration sensors using poly-crystalline silicon as sacrificial and encapsulation layer *Sensors Actuators A* **114** 355–61
- [20] Lebouitz K S, Mazaheri A, Howe R T and Pisano A 1999 Vacuum encapsulation of resonant devices using permeable polysilicon *Tech. Dig. IEEE Int. Conf. on Micro Electro Mechanical Systems* pp 470–5
- [21] He R and Kim C J 2007 On-wafer monolithic encapsulation by surface micromachining with porous polysilicon shell *J. Microelectromech. Syst.* **16** 462–72
- [22] He R and Kim C J 2006 A low temperature vacuum package utilizing porous alumina thin film encapsulation *Tech. Dig. IEEE Int. Conf. on Micro Electro Mechanical Systems (Istanbul, 22–26 January)* pp 126–9
- [23] He R and Kim C J 2009 Low-temperature monolithic encapsulation using porous-alumina shell anodized on chip *J. Microelectromech. Syst.* **18** 588–96
- [24] Verheijden G J A M, Kooops G E J, Phan K L and Van Beek J T M 2008 Wafer level encapsulation technology for MEMS devices using an HF-permeable PECVD SiOC capping layer *Tech. Dig. IEEE Int. Conf. on Micro Electro Mechanical Systems (Tucson, AZ, 13–17 January 2008)* pp 798–801
- [25] Reuter D, Bertz A, Nowack M and Gessner T 2008 Thin film encapsulation technology for harms using sacrificial CF-polymer *Sensors Actuators A* **145–6** 316–22
- [26] Pourkamali S and Ayazi F 2007 Wafer-level encapsulation and sealing of electrostatic HARPSS transducers *Proc. IEEE Sensors* 49–52
- [27] Duemling M *et al* 2006 Properties of PECVD-Oxide sealing layers in vacuum packages utilizing substrate transfer *4th*

- European Microelectronics and packaging symposium EMPS (Terme Catez, Slovenia, 22–24 May 2006)* pp 191–6
- [28] Li Q, Goosen J F L, Van Beek J T M, Van Keulen F, Phan K L and Zhang G Q 2008 Failure analysis of a thin-film nitride MEMS package *J. Microelectron. Reliab.* **48** 1557–61
- [29] Li Q, Goosen J F L, Van Beek J T M, Van Keulen F, Phan K L, Van Velzen B, Bontemps J J M, Koning J J and Zhang G Q 2008 Hermeticity and thermal stability testing of PECVD silicon nitride thin-film packages *Int. Conf. on Electronics Packaging (Japan, June 2008)* pp 220–5
- [30] Joseph P J, Monajemi P, Ayazi F and Kohl P A 2007 Wafer-level packaging of micromechanical resonators *IEEE Trans. Adv. Packag.* **30** 19–26
- [31] Monajemi P, Joseph P J, Kohl P A and Ayazi F 2005 A low cost wafer-level MEMS packaging technology *Tech. Dig. IEEE Int. Conf. on Micro Electro Mechanical Systems (30 January–3 February 2005)* pp 634–7
- [32] Monajemi P, Joseph P J, Kohl P A and Ayazi F 2006 Wafer-level MEMS packaging via thermally released metal-organic membranes *J. Micromech. Microeng.* **16** 742–50
- [33] Stark B H and Najafi K 2004 A low temperature thin-film electroplated metal vacuum package *J. Microelectromech. Syst.* **13** 147–57
- [34] Franosch M, Oppermann K G, Meckes A, Nessler W and Aigner R 2004 Wafer-level-package for bulk acoustic wave (BAW) filters *IEEE MTT-S Int. Microwave Symp. Digest (6–11 June 2004)* vol 2, pp 493–6
- [35] Seetharaman K, Van Velzen B, Van Wingerden J, Van Zadelhoff H, Yuan C, Rietveld F, Tak C, Van Beek J T M, Magnée P H C and Beijerinck H C W 2010 A robust thin-film wafer-level packaging approach for MEMS devices *Conf. IMAPS Device Packaging (Scottsdale, AZ)* p 8
- [36] Candler R N, Hopcroft M A, Kim B, Park W T, Melamud R, Agarwal M, Yama G, Partridge A, Lutz M and Kenny T W 2006 Long-term and accelerated life testing of a novel single-wafer vacuum encapsulation for MEMS resonators *J. Microelectromech. Syst.* **15** 1446–56
- [37] Kim B, Candler R N, Melamud R, Hopcroft M A, Yoneoka S, Lee H K, Agarwal M, Chandorkar S A, Yama G and Kenny T W 2009 Hermeticity and diffusion investigation in polysilicon film encapsulation for microelectromechanical systems *J. Appl. Phys.* **105** 013514
- [38] Candler R N, Park W T, Hopcroft M, Kim B and Kenny T W 2005 Hydrogen diffusion and pressure control of encapsulated MEMS resonators *13th Int. Conf. on Solid-State Sensors, Actuators and Microsystems (Seoul, 5–9 June 2005)* pp 920–3
- [39] Kim B, Candler R N, Hopcroft M A, Agarwal M, Park W T and Kenny T W 2007 Frequency stability of wafer-scale film encapsulated silicon based MEMS resonators *Sensors Actuators A* **136** 125–31
- [40] Lutz M, McDonald J, Gupta P, Partridge A, Dimpel C and Petersen K 2007 New MEMS timing references for automotive applications *Advanced Microsystems for Automotive Applications* (Berlin: Springer)
- [41] Lutz M, Partridge A, Gupta P, Buchan N, Klaassen E, McDonald J and Petersen K 2007 MEMS oscillators for high volume commercial applications *Proc. Transducers 2007* pp 49–52
- [42] Weigold J W, Wong A C, Nguyen C T and Pang S W 1999 A merged process for thick single-crystal Si resonators and BiCMOS circuitry *J. Microelectromech. Syst.* **8** 221–8
- [43] Lopez J L, Verd J, Teva J, Murillo G, Giner J, Torres F, Uranga A, Abadal G and Barniol N 2009 Integration of RF-MEMS resonators on submicrometric commercial CMOS technologies *J. Micromech. Microeng.* **19** 015002
- [44] Lo C C and Fedder G K 2007 On-chip high quality factor CMOS-MEMS silicon-fin resonators *Proc. Transducers 2007* pp 2449–52
- [45] Franke A E, Heck J M, King T J and Howe R T 2003 Polycrystalline silicon–germanium films for integrated microsystems *J. Microelectromech. Syst.* **12** 160–71
- [46] Claes G, Severi S, Van Hoof R, Decoutere S, Celis J P and Witvrouw A 2010 Influence of the novel anchor design on the shear strength of poly-sige thin film wafer level packages *IEEE 23rd Int. Conf. on Micro Electro Mechanical Systems (MEMS) (24–28 January 2010)* pp 512–5
- [47] Naito Y, Helin P, Nakamura K, De Coster J, Guo B, Haspeslagh L, Onishi K and Tilmans H A C 2010 High-Q torsional mode Si triangular beam resonators encapsulated using SiGe thin film *Proc. IEDM 2010* 154–7
- [48] Huang W L, Li S S, Ren Z and Nguyen C T C 2007 UHF nickel micro-mechanical spoke-supported ring resonators *Proc. Transducers 2007* pp 323–4
- [49] Dubois M A, Carpentier J F, Vincent P, Billard C, Parat G, Muller C, Ancey P and Conti P 2006 Monolithic above-IC resonator technology for integrated architectures in mobile and wireless communication *IEEE J. Solid-State Circuits* **41** 7–16
- [50] Newell W E 1968 Miniaturization of tuning forks *Science* **161** 1320–6
- [51] Vitzo E 2010 *Low-Power Crystal and MEMS Oscillators* (Berlin: Springer)
- [52] Mattila T, Oja A, Seppä H and Jaakola O 2002 Micromechanical bulk acoustic wave resonator *IEEE Ultrasonics Symp.* pp 945–8
- [53] Zuo C, Sinha N, Van der Spiegel J and Piazza G 2008 Multi-frequency pierce oscillators based on piezoelectric AlN contour-mode MEMS resonators *IEEE Int. Frequency Control Symp.* pp 402–7
- [54] Vitzo E A, Degrauwe M G R and Bitz S 1988 High performance crystal oscillator circuits: theory and application *IEEE J. Solid-State Circuits* **23** 774–83
- [55] Bienstman J, Tilmans H A C, Peeters E J E A, Steyaert M and Puers R 1996 An oscillator circuit for electrostatically driven silicon-based one-port resonators *Sensors Actuators A* **52** 179–86
- [56] Leeson D B 1965 A simple model of feedback oscillator noise spectrum *Proc. IEEE* pp 329–30
- [57] He L, Xu Y P and Palaniapan M 2010 A state-space phase-noise model for nonlinear MEMS oscillators employing automatic amplitude control *IEEE Trans. Circuits Syst. I* **57** 189–99
- [58] Hajimiri A and Lee T H 1998 A general theory of phase noise in electrical oscillators *IEEE J. Solid-State Circuits* **33** 179–94
- [59] Lee T H and Hajimiri A 2000 Oscillator phase noise: a tutorial *IEEE J. Solid-State Circuits* **35** 326–36
- [60] Kaajakari V, Koskinen J K and Mattila T 2005 Phase noise in capacitively coupled micromechanical oscillators *IEEE Trans. Ultrason. Ferroelectr. Freq. Control* **52** 2322–31
- [61] Roessig T A, Howe R T and Pisano A P 1997 Nonlinear mixing in surface-micromachined tuning fork oscillators *IEEE Int. Frequency Control Symp.* pp 778–82
- [62] Lin Y W, Lee S, Ren Z and Nguyen C T C 2003 Series-resonant micromechanical resonator oscillator *Tech. Dig. IEEE Int. Electron Devices Meeting, IEDM'03* 39.4.1–4
- [63] Agarwal M, Park K K, Hopcroft M, Chandorkar S, Candler R N, Kim B, Melamud R, Yama G, Murmann B and Kenny T W 2006 Effects of mechanical vibrations and bias voltage noise on phase noise of MEMS resonator based oscillators *Proc. MEMS 2006 (Istanbul, 22–26 January 2006)* pp 154–7



- [64] Vig J R 1999 Noise in microelectromechanical system resonators *IEEE Trans. Ultrason. Ferroelectr. Freq. Control* **46** 1558–65
- [65] Lin Y-W, Lee S, Li S, Xie Y, Ren Z and Nguyen C T-C 2004 Series-resonant VHF micromechanical resonator reference oscillators *IEEE J. Solid-State Circuits* **39** 2477–90
- [66] Lee S and Nguyen C T-C 2004 Mechanically-coupled micromechanical resonator arrays for improved phase noise *Proc. IEEE Int. Frequency Control Symp. and Exposition* pp 144–50
- [67] Akgul M, Kim B, Hung L W, Lin Y, Li W-C, Huang W-L, Gurin I, Borna A and Nguyen C T-C 2009 Oscillator far-from carrier phase noise reduction via nano-scale gap tuning of micromechanical resonators *Solid-State Sensors, Actuators and Microsystems Conf., Transducers 2009* pp 798–801
- [68] Egan W F 1990 Modeling phase noise in frequency dividers *IEEE Trans. Ultrason. Ferroelectr. Freq. Control* **37** 307–15
- [69] SenGupta A and Walls F L 2000 Effect of aliasing on spurs and PM noise in frequency dividers *Proc. IEEE/EIA Int. Frequency Control Symp. and Exhibition* pp 541–8
- [70] Chandralahim H, Bhavé S A, Quévy E P and Howe R T 2007 Aqueous transduction of poly-SiGe disk resonators *Proc. Transducers 2007* pp 313–6
- [71] Lakin K M 2003 A review of thin-film resonator technology *IEEE Microwave Magazine* **4** 61–7
- [72] Piazza G, Abdolvand R, Ho G K and Ayazi F 2004 Voltage-tunable piezoelectrically-transduced single-crystal silicon micromechanical resonators *Sensors Actuators A* **111** 71–8
- [73] Vanhelmont F, Philippe P, Jansman A B M, Milsom R F, Ruigrok J J M and Oruk A 2006 A 2 GHz reference oscillator incorporating a temperature compensated BAW resonator *IEEE Ultrasonics Symp.* pp 333–6
- [74] Mareschal O, Loiseau S, Verjus F, Valbin L, Lissorgues G, Bouregba R, Poullain G, Saez S and Dolabdjian C 2009 Modeling and fabrication of piezoelectric aluminum nitride resonator and its application in oscillators *Proc. Transducers 2009* pp 565–8
- [75] Wojciechowski K E, Olsson R H III, Tuck M R, Roherty-Osmun E and Hill T A 2009 Single-chip precision oscillators based on multi-frequency, high-Q aluminium nitride MEMS resonators *Proc. Transducers 2009* pp 2126–30
- [76] Abdolvand R and Farrokhi A 2007 Enhanced power handling and quality factor in thin-film piezoelectric-on-substrate resonators *IEEE Ultrasonics Symp.* pp 608–11
- [77] Abdolvand R, Lavasani H M, Ho G K and Ayazi F 2008 Thin-film piezoelectric-on-silicon resonators for high-frequency reference oscillator applications *IEEE Trans. Ultrason. Ferroelectr. Freq. Control* **55** 2596–606
- [78] Sepúlveda N, Lu J, Aslam D M and Sullivan J P 2008 High-performance polycrystalline diamond micro- and nanoresonators *J. Microelectromech. Syst.* **17** 473–82
- [79] Bhavé S A and Howe R T 2004 Internal electrostatic transduction for bulk-mode MEMS resonators *Solid-State Sensor, Actuator and Microsystems Workshop (Hilton Head Island, SC, 6–10 June 2004)* pp 59–60
- [80] Weinstein D, Chandralahim H, Cheow L F and Bhavé S A 2006 Dielectrically transduced single-ended to differential MEMS filter *Proc. ISSCC* 318–9
- [81] Ransley J H T, Aziz A, Durkan C and Seshia A A 2008 Silicon depletion layer actuators *Appl. Phys. Lett.* **92** 184103
- [82] Hwang E and Bhavé S A 2010 PN-diode transduced 3.7-GHz silicon resonator *23rd IEEE Int. Conf. on Micro Electro Mechanical Systems (MEMS 2010)* pp 208–11
- [83] Piazza G Piezoelectric aluminum nitride vibrating RF MEMS for radio front-end technology 2005 Thesis University of California, Berkeley
- [84] Dubois M-A and Muralt P 1999 Properties of aluminum nitride thin films for piezoelectric transducers and microwave filter applications *Appl. Phys. Lett.* **74** 3032–4
- [85] Kaajakari V, Alastalo A T and Mattila T 2006 Electrostatic transducers for micromechanical resonators: free space and solid dielectric *IEEE Trans. Ultrason. Ferroelectr. Freq. Control* **53** 2484–9
- [86] Weinstein D and Bhavé S A 2009 Internal dielectric transduction in bulk-mode resonators *J. Microelectromech. Syst.* **18** 1401–8
- [87] Weinstein D and Bhavé S A 2007 Internal dielectric transduction: optimal position and frequency scaling *IEEE Trans. Ultrason. Ferroelectr. Freq. Control* **54** 2696–8
- [88] Samrao A K and Ayazi F 2010 Self-polarized capacitive silicon micromechanical resonators via charge trapping *Proc. IEDM 2010* 166–9
- [89] Pourkamali S, Ho G K and Ayazi F 2007 Low-impedance VHF and UHF capacitive silicon bulk acoustic wave resonators: part I. Concept and fabrication *IEEE Trans. Electron Devices* **54** 2017–23
- [90] Clark J R, Hsu W-T and Nguyen C T-C 2000 High-Q VHF micromechanical contour-mode disk resonators *Technical Digest, IEEE Int. Electron Devices Meeting (San Francisco, CA, 11–13 December 2000)* pp 493–6
- [91] Kiihamaki J, Kaajakari V, Luoto H, Kattelus H and Yli-Koski M 2005 Fabrication of single crystal silicon resonators with narrow gaps *Proc. Transducers V2* pp 1354–57
- [92] Hsu W-T, Clark J R and Nguyen C T-C 2001 A sub-micron capacitive gap process for multiple-metal-electrode lateral micromechanical resonators *Tech. Dig. IEEE Int. Micro Electro Mechanical Systems Conf. (Interlaken, Switzerland, 21–25 January 2001)* pp 349–52
- [93] Yoel S and Ayazi F 2001 The HARPSS process for fabrication of nano-precision silicon electromechanical resonators *IEEE Proc. 2001 1st IEEE Conf. on Nanotechnology* pp 489–94
- [94] Galayko D, Kaiser A, Buchaillet L, Legrand B, Collard D and Combi C 2003 Design, realization and testing of micro-mechanical resonators in thick-film silicon technology with postprocess electrode-to-resonator gap reduction *J. Micromech. Microeng.* **13** 134–40
- [95] Pourkamali S and Ayazi F 2004 Fully single crystal silicon resonators with deep-submicron dry-etched transducer gaps *17th IEEE Int. Conf. on Micro Electro Mechanical Systems (MEMS)* pp 813–6
- [96] Pourkamali S, Hashimura A, Abdolvand R, Ho G K, Erbil A and Ayazi F 2003 High-Q single crystal silicon HARPSS capacitive beam resonators with self-aligned sub-100-nm transduction gaps *J. Micromech. Syst.* **12** 487–96
- [97] Abdolvand R and Ayazi F 2005 Single-mask reduced-gap capacitive micromachined devices *18th IEEE Int. Conf. on Micro Electro Mechanical Systems (MEMS)* pp 151–4
- [98] Kiihamäki J, Kaajakari V, Luoto H, Kattelus H and Yli-Koski M 2005 Fabrication of single crystal silicon resonators with narrow gaps *13th Int. Conf. on Solid-State Sensors, Actuators and Microsystems (Seoul, Korea, 5–9 June 2005)* pp 1354–7
- [99] Ferri M, Mancarella F, Roncaglia A, Ransley J, Yan J and Seshia A 2008 Fabrication of DETF sensors in SOI technology with submicron air gaps using a maskless line narrowing technique *IEEE Sensors (26–29 October 2008)* pp 1131–4
- [100] Stoffels S, Bryce G, Van Hoof R, Du Bois B, Mertens R P, Puers R, Tilmans H and Witvrouw A 2009 A novel gap narrowing process for extremely thin, high aspect ratio transduction gaps for MEMS HF Resonators *Mater. Res. Soc. Symp. Proc.* **1139** 13–8

- [101] Samara A K and Ayazi F 2011 Combined capacitive and piezo-electric transduction for high performance silicon microresonators *Proc. MEMS 2011* pp 169–72
- [102] Lin A T-H, Lee J E-Y, Yan J and Seshia A A 2009 Enhanced transduction methods for electrostatically driven MEMS resonators *Int. Solid-State Sensors, Actuators and Microsystems Conference, Transducers 2009 (21–25 June 2009)* pp 561–4
- [103] Lee J E-Y and Seshia A A 2008 Enhanced electrical characterization of MEMS resonators using on-chip parasitic feedthrough self-cancellation *Proc. Eurosensors XXII* pp 1349–52
- [104] Lee J E-Y, Bahreyni B, Yong Z and Seshia A A 2008 A single-crystal-silicon bulk-acoustic-mode microresonator oscillator *IEEE Electron Device Lett.* **29** 701–3
- [105] Ruffieux D, Krummenacher F, Pezous A and Spinola-Durante G 2010 Silicon resonator based 3.2  $\mu$ W real time clock with 10 ppm frequency accuracy *IEEE J. Solid-State Circuits* **45** 224–34
- [106] Zuo C, Sinha N, Van der Spiegel J and Piazza G 2010 Multifrequency pierce oscillators based on piezoelectric AlN contour-mode MEMS technology *J. Microelectromech. Syst.* **19** 570–80
- [107] Zuo C, Van Der Spiegel J and Piazza G 2010 1.05-GHz CMOS oscillator based on lateral-field-excited piezoelectric AlN contour-mode MEMS resonators *IEEE Trans. Ultrason. Ferroelectr. Freq. Control* **57** 82–7
- [108] Abdolvand R, Lavasani H, Ho G and Ayazi F 2008 Thin-film piezoelectric-on-silicon resonators for high-frequency reference oscillator applications *IEEE Trans. Ultrason. Ferroelectr. Freq. Control* **55** 2596–606
- [109] Lavasani H M, Wanling P and Ayazi F 2010 An electronically temperature-compensated 427 MHz low phase-noise AlN-on-Si micromechanical reference oscillator *IEEE Radio Frequency Integrated Circuits Symp. (RFIC)* pp 329–32
- [110] Lavasani H M, Abdolvand R and Ayazi F 2008 Low phase-noise UHF thin-film piezoelectric-on-substrate LBAR oscillators *IEEE 21st Int. Conf. on Micro Electro Mechanical Systems, MEMS 2008* pp 1012–5
- [111] Lavasani H M, Abdolvand R and Ayazi F 2007 A 500 MHz low phase-noise AlN-on-silicon reference oscillator *IEEE Custom Integrated Circuits Conf., CICC'07* pp 599–602
- [112] Hu J, Callaghan L, Ruby R and Otis B 2010 A 50 ppm 600 MHz frequency reference utilizing the series resonance of an FBAR *IEEE Radio Frequency Integrated Circuits Symp. (23–25 May 2010)* pp 325–8
- [113] Lavasani H M, Wanling P, Harrington B, Abdolvand R and Ayazi F 2010 A 76 dB $\Omega$  1.7 GHz 0.18  $\mu$ m CMOS tunable transimpedance amplifier using broadband current pre-amplifier for high frequency lateral micromechanical oscillators *IEEE Int. Solid-State Circuits Conf. Digest of Technical Papers (ISSCC)* pp 318–9
- [114] Nguyen C T-C and Howe R T 1999 An integrated CMOS micromechanical resonator high-Q oscillator *IEEE J. Solid-State Circuits* **34** 440–55
- [115] Cioffi K R and Hsu W-T 2005 32 kHz MEMS-based oscillator for low-power applications *Proc. 2005 IEEE Int. Frequency Control Symp. and Exposition* pp 551–8
- [116] Roessig T A, Howe R T and Pisano A P 1998 Surface-micromachined 1 MHz oscillator with low-noise Pierce configuration *Proc. Solid State Sensor and Actuator Workshop (Hilton Head, SC, 1 June 1998)*
- [117] Lee J E-Y and Seshia A A 2008 Square wine glass mode resonator with quality factor of 4 million *IEEE Sensors (26–29 October 2008)* pp 1257–60
- [118] Henry R and Kenny D 2008 Comparative analysis of MEMS, programmable, and synthesized frequency control devices versus traditional quartz based devices *IEEE Freq. Control Symp.* pp 396–401
- [119] Lee J E-Y and Seshia A A 2008 Circular wine glass mode disk resonator with Q of 2 million *Proc. Eurosensors XXII* pp 277–9
- [120] Khine L, Palaniapan M and Wong W-K 2007 6 MHz bulk-mode resonator with Q values exceeding one million *Proc. Transducers 2007* pp 2445–8
- [121] Lee S, Demirci M U and Nguyen C T-C 2001 A 10-MHz micromechanical resonator Pierce reference oscillator for communications *Tech. Dig. 11th Int. Conf. on Solid-State Sensors and Actuators (Transducers'01) (Munich, Germany, 10–14 June 2001)* pp 1094–7
- [122] Mattila T, Kiihamäki J, Lamminmäki T, Jaakkola O, Rantakari P, Oja A, Seppä H, Kattelus H and Tittonen I A 12 MHz micromechanical bulk acoustic mode oscillator *Sensors Actuators A* **101** 1–9
- [123] Rantakari P, Kaajakari V, Mattila T, Kiihamoki J, Oja A, Tittonen I and Seppo H 2005 Low noise, low power micromechanical oscillator *13th International Conference on Solid-State Sensors, Actuators and Microsystems (Seoul, 5–9 June 2005)* pp 2135–8
- [124] Kaajakari V, Mattila T, Oja A, Kiihamäki J and Seppä H 2004 Square-extensional mode single-crystal silicon micromechanical resonator for low-phase-noise oscillator applications *IEEE Electron Device Lett.* **25** 173–5
- [125] Kaajakari V, Mattila T, Oja A, Kiihamoki J, Kattelus H, Koskenvuori M, Rantakari P, Tittonen I and Seppo H 2003 Square-extensional mode single-crystal silicon micromechanical RF-resonator *12th Int. Conf. on Solid State Sensors, Actuators and Microsystems (Boston, MA, 8–12 June 2003)* pp 951–4
- [126] Mattila T, Jaakkola O, Kiihamäki J, Karttunen J, Lamminmäki T, Pantakari P, Oja A, Seppä H, Kattelus H and Tittonen I 14 MHz micromechanical oscillator *Sensors Actuators A* **3204** 1–6
- [127] Sworowski M, Neuilly F, Legrand B, Summanwar A, Philippe P and Buchaillet L 2010 Fabrication of 24-MHz-disk resonators with silicon passive integration technology *IEEE Electron Device Lett.* **31** 23–5
- [128] Lin Y-W, Lee S, Li S-S, Xie Y, Ren Z and Nguyen C T-C 2004 60-MHz wine-glass micromechanical-disk reference oscillator *ISSCC 2004 (18 February 2004)* **1** 322–530
- [129] Pourkamali S, Ho G K and Ayazi F 2007 Low-impedance VHF and UHF capacitive silicon bulk acoustic-wave resonators—part II. Measurement and characterization *IEEE Trans. Electron Devices* **54** 2024–30
- [130] Sundaresan K, Ho G K, Pourkamali S and Ayazi F 2006 A low phase noise 100 MHz silicon BAW reference oscillator *IEEE Custom Integrated Circuits Conference, CICC'06* pp 841–4
- [131] Lavasani H M, Samara A K, Casinovi G and Ayazi F 2008 A 145 MHz low phase-noise capacitive silicon micromechanical oscillator *Proc. IEDM 2008* pp 675–8
- [132] Xie Y, Li S, Lin Y, Ren Z and Nguyen C T 2003 UHF Micromechanical extensional wine-glass mode ring resonators *Proc. IEDM 2003* pp 39.2.1–4
- [133] Ziaei-Moayyed M, Hsieh J, Chen J-W P, Quévy E P, Elata D and Howe R T 2009 Higher-order mode internal electrostatic transduction of a bulk-mode ring resonator on a quartz substrate *Int. Solid-State Sensors, Actuators and Microsystems Conf. (Transducers)* pp 2338–41
- [134] Kaajakari V, Mattila T, Oja A and Seppo H 2004 Nonlinear limits for single-crystal silicon microresonators *J. Microelectromech. Syst.* **13** 715–24
- [135] Mestrom R M C, Fey R H B, Van Beek J T M, Phan K L and Nijmeijer H 2007 Modelling the dynamics of a MEMS resonator: simulations and experiments *Sensors Actuators A* **142** 306–15



- [136] Agarwal M, Park K, Candler R, Hopcroft M, Jha C, Melamud R, Kim B, Murmann B and Kenny T W 2005 Non-linearity cancellation in MEMS resonators for improved power-handling *IEDM Technical Digest IEEE International Electron Devices Meeting* pp 286–9
- [137] Kaajakari V, Mattila T, Kiihamaki J, Kattelus H, Oja A and Seppa H 2003 Nonlinearities in single-crystal silicon micromechanical resonators *12th Int. Conf. on Solid State Sensors, Actuators and Microsystems (Boston, MA, 8–12 June 2003)* pp 1574–7
- [138] Nosek J 1999 Drive level dependence of the resonant frequency in BAW quartz resonators and his modeling *IEEE Trans. Ultrason. Ferroelectr. Freq. Control* **46** 823–9
- [139] Pardo M, Sorenson L, Pan W and Ayazi F 2011 Phase noise shaping via forced nonlinearity in piezoelectrically actuated silicon micromechanical oscillators *Proc. MEMS 2011* pp 780–3
- [140] Kubena R L, Stratton F P, Chang D T, Joyce R J, Hsu T Y, Lim M K and Closkey R T M 2005 MEMS-based quartz oscillators and filters for on-chip integration *Proc. 2005 IEEE Int. Frequency Control Symp. and Exposition* pp 122–7
- [141] Phan K L, Van Beek J T M and Koops G E J 2009 Piezoresistive ring-shaped MEMS resonator *Int. Solid-State Sensors, Actuators and Microsystems Conf. (Transducers) (21–25 June 2009)* pp 1413–6
- [142] Van der Avoort C, Van der Hout R, Bontemps J J M, Steeneken P G, Le Phan K, Fey R H B, Hulshof J and van Beek J T M 2010 Amplitude saturation of MEMS resonators explained by autoparametric resonance *J. Micromech. Microeng.* **20** 105012
- [143] van der Avoort C, van der Hout R and Hulshof J 2011 Parametric resonance and Hopf bifurcation analysis for a MEMS resonator *Physica D* **240** 913–9
- [144] Weinberg M, Candler R, Chandorkar S, Varsanik J, Kenny T and Duwel A 2009 Energy loss in MEMS resonators and the impact on inertial and RF devices *Int. Solid-State Sensors, Actuators and Microsystems Conf. (Transducers)* pp 688–95
- [145] Wang J, Butler J E, Feygelson T and Nguyen C T-C 2004 1.51-GHz nanocrystalline diamond micromechanical disk resonator with material-mismatched isolating support *Proc. MEMS 2004* pp 641–4
- [146] Lee J E-Y, Yan J and Seshia A A 2008 Quality factor enhancement of bulk acoustic resonators through anchor geometry design *Proc. Eurosensors XXII* pp 536–9
- [147] Blom F R, Bouwstra S, Elwenspoek M and Fluittsma J H J 1992 Dependence of the quality factor of micromachined silicon beam resonators on pressure and geometry *J. Vac. Sci. Technol. B* **10** 19–26
- [148] Suijlen M A G, Van Beek J T M, Koning J J and Beijerinck H C W Model-based design of MEMS resonant pressure sensors *PhD thesis Technische Universiteit Eindhoven*
- [149] Yasumura K Y, Stowe T D, Chow E M, Pfafman T, Kenny T W, Stipe B C and Rugar D 2000 Quality factors in micron and submicron-thick cantilevers *IEEE/ASME J. Microelectromech. Syst.* **9** 117–25
- [150] Roszhart T V 1990 The effect of thermoelastic internal friction on the  $Q$  of micromachined silicon resonators *IEEE 4th Technical Digest Solid-State Sensor and Actuator Workshop* pp 13–6
- [151] Tabrizian R, Rais-Zadeh M and Ayazi F 2009 Effect of phonon interactions on limiting the  $f \cdot Q$  product of micromechanical resonators *Int. Solid-State Sensors, Actuators and Microsystems Conf. (Transducers)* pp 2131–4
- [152] Chandorkar S A, Agarwal M, Melamud R, Candler R N, Goodson K E and Kenny T W 2008 Limits of quality factor in bulk-mode micromechanical resonators *IEEE 21st Int. Conf. on Micro Electro Mechanical Systems (MEMS 2008)* pp 74–7
- [153] McClelland T, Stone C and Bloch M 1999 100 MHz crystal oscillator with extremely low phase noise *Proc. Joint Meeting of the European Frequency and Time Forum and the IEEE International Frequency Control Symp.* vol **1**, pp 331–4
- [154] Kim B, Hopcroft M A, Candler R N, Jha C M, Agarwal M, Melamud R, Chandorkar S A, Yama G and Kenny T W 2008 Temperature dependence of quality factor in MEMS resonators *J. Micromech. Syst.* **17** 755–66
- [155] Li W-C, Lin Y, Kim B, Ren Z and Nguyen C T-C 2009 Quality factor enhancement in micromechanical resonators at cryogenic temperatures *Int. Solid-State Sensors, Actuators and Microsystems Conf., Transducers'09* pp 1445–8
- [156] Badila-Ciressan N D, Mazza M, Grogg D and Ionescu A M 2007 Fragmented membrane MEM bulk lateral resonators with nano-gaps on 1.5  $\mu\text{m}$  SOI *37th European Solid State Device Research Conference ESSDERC 2007* pp 430–3
- [157] Hwang E and Bhawe S A 2010 Low temperature quality factor scaling of GHz frequency silicon resonators *Solid State Sensor, Actuator and Microsystems Workshop (Hilton Head Island, SC, 6–10 June 2010)* pp 388–9
- [158] Ziaei-Moayyed M, Habermehl S D, Branch D W, Clews P J and Olsson R H 2011 Silicon Carbide lateral overtone bulk acoustic resonator with ultra-high quality factor *Proc. MEMS 2011 (Cancun, Mexico, 23–7 January 2011)* pp 788–92
- [159] Khine L and Palaniapan M 2009 High-Q bulk-mode SOI square resonators with straight-beam anchors *J. Micromech. Microeng.* **19** 015017
- [160] Wang J, Ren Z and Nguyen C T-C 2004 1.156-GHz self-aligned vibrating micromechanical disk resonator *IEEE Trans. Ultrason. Ferroelectr. Freq. Control* **51** 1607–28
- [161] Hung L-W and Nguyen C T-C 2010 Q-boosted AlN array-composite resonator with  $Q > 10\,000$  *IEEE International Electron Devices Meeting (IEDM)* pp 7.3.1–4
- [162] Hung L-W and Nguyen C T-C 2011 Capacitive-piezoelectric AlN resonators with  $Q > 12\,000$  *Proc. MEMS 2011 (Cancun, Mexico, 23–27 January 2011)* pp 173–6
- [163] Kuypers J H, Zolfagharkhani G, Gaidarzhy A, Rebel R, Chen D M, Stanley S, LoCasio D, Schoepf K J, Crowley M and Mohanty P 2010 High performance MEMS oscillators for communications applications *4th Int. Symp. on Acoustic Wave Devices (Chiba University, March 2010)*
- [164] Hegazi E, Sjolund H and Abidi A A 2001 A filtering technique to lower LC oscillator phase noise *IEEE J. Solid-State Circuits* **36** 1921–30
- [165] Tiebout M 2001 Low-power low-phase-noise differentially tuned quadrature VCO design in standard CMOS *IEEE J. Solid-State Circuits* **36** 1018–24
- [166] Margarit M A, Joo L T, Meyer R G and Deen M J 1999 A low-noise, low-power VCO with automatic amplitude control for wireless applications *IEEE J. Solid-State Circuits* **34** 761–71
- [167] Hajimiri A and Lee T H 1998 Phase noise in CMOS differential LC oscillators *Tech. Dig. Symp. on VLSI Circuits (11–13 June 1998)* pp 48–51
- [168] Nathanson H C, Newell W E, Wickstrom R A and Davis J R Jr 1967 The resonant gate transistor *IEEE Trans. Electron Devices* **ED-14** 117–33
- [169] Grogg D, Mazza M, Tsamados D and Ionescu A M 2008 Multi-gate vibrating-body field effect transistor (VB-FETs) *Proc. IEDM 2008* pp 663–6

- [170] Weinstein D and Bhavé S A 2010 The resonant body transistor *Nano Lett.* **10** 1234–7
- [171] Bartsch S T, Grogg D, Lovera A, Tsamados D, Ayöz S and Ionescu Adrian M 2010 Resonant-body Fin-FETs with sub-nW power consumption *IEEE Int. Electron Devices Meeting (IEDM)* pp 7.6.1–4
- [172] Grogg D, Ayöz S and Ionescu A M 2009 Self-sustained low power oscillator based on vibrating body field effect transistor *IEEE Int. Electron Devices Meeting (IEDM)* pp 1–4
- [173] Van Beek J T M, Steeneken P G and Giesbers B 2006 A 10 MHz piezoresistive MEMS resonator with high Q *IEEE Int. Frequency Control Symp. and Exposition (4–7 June 2006)* pp 475–80
- [174] Van Beek J T M, Le Phan K, Verheijden G J A M, Koops G E J, Van der Avoort C, Van Wingerden J, Ernur Badaroglu D, Bontemps J J M and Puers R 2008 A piezo-resistive resonant MEMS amplifier *IEEE Int. Electron Devices Meeting, IEDM 2008* vol 1–4, pp 667–70
- [175] Van Beek J T M, Verheijden G J A M, Koops G E J, Le Phan K, Van der Avoort C, Van Wingerden J, Badaroglu Ernur D and Bontemps J J M 2007 Scalable 1.1 GHz fundamental mode piezo-resistive silicon MEMS resonator *IEEE Int. Electron Devices Meeting, IEDM (10–12 December 2007)* pp 411–4
- [176] Wang W, Popa L C, Marathe R and Weinstein D 2011 An unreleased mm-wave resonant body transistor *Proc. MEMS 2011* pp 1341–4
- [177] Steeneken P G, Le Phan K, Goossens M J, Koops G E J, Brom G J A M, Van der Avoort C and Van Beek J T M 2011 Piezoresistive heat engine and refrigerator *Nature Phys.* **7** 354–9
- [178] Reichenbach R B, Zalalutdinov M, Parpia J M and Craighead H G 2006 RF MEMS oscillator with integrated resistive transduction *IEEE Electron Device Lett.* **27** 805–7
- [179] Seo J H and Brand O 2008 High Q-factor in-plane-mode resonant microsensor platform for gaseous/liquid environment *J. Microelectromech. Syst.* **17** 483–93
- [180] Rahafrooz A and Pourkamali S 2010 Fully micromechanical piezo-thermal oscillators *IEEE Int. Electron Devices Meeting (IEDM)* pp 7.2.1–4
- [181] Rahafrooz A and Pourkamali S 2011 Active self-Q-enhancement in high frequency thermally actuated M/NEMS resonators *Proc. MEMS 2011 (Cancun, 23–27 January 2011)* pp 760–3
- [182] Hajjam A, Rahafrooz A and Pourkamali S 2011 Temperature compensated single-device electromechanical oscillators *Proc. MEMS 2011 (Cancun, 23–27 January 2011)* pp 801–4
- [183] Bontemps J J M *et al* 2009 56 MHz piezoresistive micromechanical oscillator *Int. Solid-State Sensors, Actuators and Microsystems Conf., Transducers'09 (21–25 June 2009)* pp 1433–6
- [184] Sundaresan K, Ho G K, Pourkamali S and Ayazi F 2007 Electronically temperature compensated silicon bulk acoustic resonator reference oscillators *IEEE J. Solid-State Circuits* **42** 1425–34
- [185] Koskenvuo M, Kaajakari V, Mattila T and Tittonen I 2008 Temperature measurement and compensation based on two vibrating modes of a bulk acoustic mode micro resonator *IEEE 21st Int. Conf. on Micro Electro Mechanical Systems, MEMS 2008 (Tucson, AZ, 13–17 January 2008)* pp 78–81
- [186] Salvia J, Melamud R, Lee H K, Qu Y Q, Lord S F, Murmann B and Kenny T W 2009 Phase lock loop based temperature compensation for MEMS oscillators *Proc. MEMS 2009* pp 661–4
- [187] Lakin K M, McCarron K T and McDonald J F 2000 Temperature compensated bulk acoustic thin film resonators *IEEE Ultrasonics Symp.* pp 855–8
- [188] Abdolvand R, Mirilavasani H and Ayazi F 2007 A low-voltage temperature stable micro-mechanical piezoelectric oscillator *Proc. Transducers 2007* vol 1, pp 53–6
- [189] Sandberg R, Svendsen W, Mølhave K and Boisen A 2005 Temperature and pressure dependence of resonance in multi-layer microcantilevers *J. Micromech. Microeng.* **15** 1454–8
- [190] Melamud R, Kim B, Hopcroft A, Chandorkar S, Agarwal M, Jha C M and Kenny T W 2007 Composite flexural mode resonator with controllable turnover temperature *Proc. MEMS 2007* pp 199–202
- [191] Wang J S and Lakin K M 1982 Low-temperature coefficient bulk acoustic wave composite resonators *Appl. Phys. Lett.* **40** 308–10
- [192] Kim B, Melamud R, Hopcroft M A, Chandorkar S A, Bahl G, Messana M, Candler R N, Yama G and Kenny T 2007 Si-SiO<sub>2</sub> composite MEMS resonators in CMOS compatible wafer-scale thin-film encapsulation *IEEE Int. Frequency Control Symp., 2007 Joint with the 21st European Frequency and Time Forum* pp 1214–9
- [193] Van der Avoort C, Van Wingerden J and Van Beek J T M 2009 The effects of thermal oxidation of a MEMS resonator on temperature drift and absolute frequency *IEEE 22nd Int. Conf. on Micro Electro Mechanical Systems, MEMS 2009 (25–29 January 2009)* pp 654–6
- [194] Kalicinski S, Tilmans H A C, Wevers M and De Wolf I 2008 A new method to determine the mechanical resonance frequency, quality factor and charging in electrostatically actuated MEMS *IEEE 21st Int. Conf. on Micro Electro Mechanical Systems, MEMS 2008 (13–17 January 2008)* pp 653–6
- [195] Melamud R, Chandorkar S A, Kim B, Lee H K, Salvia J C, Bahl G, Hopcroft M A and Kenny T W 2009 Temperature-insensitive composite micromechanical resonators *J. Micromech. Syst.* **18** 1409–19
- [196] Samarao A K and Ayazi F 2009 Temperature compensation of silicon micromechanical resonators via degenerate doping *IEEE Int. Electron Devices Meeting (IEDM)* pp 1–4
- [197] Csavinsky P and Einspruch N G 1963 Effect of doping on elastic constants of silicon *Phys. Rev. A* **132** 2434–40
- [198] Samarao A K, Casinovi G and Ayazi F 2010 Passive TCF compensation in high Q silicon micromechanical resonators *Proc. MEMS 2010* pp 116–9
- [199] Samarao A K and Ayazi F 2010 Intrinsic temperature compensation of highly resistive high-Q silicon microresonators via charge carrier depletion *IEEE Int. Frequency Control Symp. (IFCS)* pp 334–9
- [200] Rai S, Ying S, Wei P, Ruby R and Otis B 2010 A digitally compensated 1.5 GHz CMOS/FBAR frequency reference *IEEE Trans. Ultrason. Ferroelectr. Freq. Control* **57** 552–61
- [201] Seo J H, Demirci K S, Byun A, Truax S and Brand O 2007 Novel temperature compensation scheme for microresonators based on controlled stiffness modulation *Proc. Transducers 2007* pp 2457–60
- [202] Hsu W-T and Nguyen C 2002 Stiffness-compensated temperature insensitive micromechanical resonators *15th IEEE Int. Conf. on Micro Electro Mechanical Systems* pp 731–4
- [203] Sundaresan K, Ho G K, Pourkamali S and Ayazi F 2005 A two-chip, 4-MHz, microelectromechanical reference oscillator *IEEE Int. Symp. on Circuits and Systems, ISCAS 2005* vol 6, pp 5461–4
- [204] Ho G K, Sundaresan K, Pourkamali S and Ayazi F 2010 Micromechanical IBARs: tunable high-Q resonators for temperature-compensated reference oscillators *J. Microelectromech. Syst.* **19** 503–15

- [205] Ho G K, Sundaesan K, Pourkamali S and Ayazi F 2005 Low motional impedance highly tunable  $I^2$  resonators for temperature compensated reference oscillators *18th IEEE Int. Conf. on Micro Electro Mechanical Systems, MEMS 2005* pp 116–20
- [206] Ruffieux D, Pezous A, Pliska A-C and Krummenacher F 2009 Silicon-resonator-based, 3.2  $\mu$ W real-time clock with  $\pm 10$  ppm frequency accuracy *Tech. Dig. IEEE Int. Solid-State Circuits Conf., ISSCC 2009 (8–12 February 2009)* pp 214–34
- [207] McCorquodale M S, Carichner G A, O'Day J D, Pernia S M, Kubba S, Marsman E D, Kuhn J J and Brown R B 2009 A 25-MHz self-referenced solid-state frequency source suitable for XO-replacement *IEEE Trans. Circuits Syst. I* **56** 943–56
- [208] McCorquodale M S, Pernia S M, O'Day J D, Carichner G, Marsman E, Nguyen N, Kubba S, Nguyen S, Kuhn J and Brown R B 2008 A 0.5-to-480 MHz self-referenced CMOS clock generator with 90 ppm total frequency error and spread-spectrum capability *Proc. ISSCC 2008* p 350
- [209] Schoepf K J, Rebel R, Chen D M, Zolfagharkhani G, Gaidarhy A, Kuypers J H, Crowley M and Mohanty P 2009 TCMO<sup>TM</sup>: a versatile MEMS oscillator timing platform *41st Annual Precise Time and Time Interval (PTTI) Meeting* pp 481–92
- [210] Smagin A G 1994 Irreversible frequency variations in time of precision quartz crystal units *48th. Proc. 1994 IEEE Int. Frequency Control Symp.* pp 541–3
- [211] Watanabe Y, Fujita N, Goka S, Sekimoto H and Uchida T 1999 Drive-level dependence of long-term aging in quartz resonators *Proc. Joint Meeting of the European Frequency and Time Forum and the IEEE International Frequency Control Symp.* vol 1, pp 397–400
- [212] Filler R L and Vig J R 1992 Long term aging of oscillators *IEEE Proc. 46th Frequency Control Symp.* pp 470–84
- [213] Vig J R and Meeker T R 1991 The aging of bulk acoustic wave resonators, filters and oscillators *IEEE Proc. 45th Annual Symp. on Frequency Control (29–31 May 1991)* pp 77–101
- [214] Koskenvuo M, Matilla T, Haara A, Tittonen I, Oja A and Seppa H 2004 Long-term stability of single-crystal silicon micro resonators *Sensors Actuators A* **115** 2327
- [215] Lakin K M, McCarron K T, McDonald J F and Belsick J 2001 Temperature coefficient and ageing of BAW composite materials *Proc. 2001 IEEE Int. Frequency Control Symp. and PDA Exhibition* pp 605–8
- [216] Kosinski J A 2000 Theory and design of crystal oscillators immune to acceleration: present state of the art *IEEE/EIA Int. Frequency Control Symp. and Exhibition* pp 260–8
- [217] Filler R L 1987 The acceleration sensitivity of quartz crystal oscillators: a review *41st Annual Frequency Control Symp.* pp 398–408
- [218] Discera product sheet [resonator\MOS1-S3-0825-na datasheet.pdf](#)
- [219] SiTime website <http://www.sitime.com/products/high-performance-programmable-oscillators.php>
- [220] Lin Y, Wang J, Pietrangelo S, Ren Z and Nguyen C T-C 2007 Effect of electrode configuration on the frequency and quality factor repeatability of RF micromechanical disk resonators *Proc. Transducers 2007* pp 2461–4
- [221] Hsu W-T and Brown A R 2007 Frequency trimming for MEMS resonator oscillators *Proc. IEEE IFCS 2007* pp 1088–91
- [222] Samarao A K and Ayazi F 2009 Post-fabrication electrical trimming of silicon bulk acoustic resonators using Joule heating *IEEE 22nd Int. Conf. on Micro Electro Mechanical Systems, MEMS 2009* pp 892–5
- [223] Chiao M and Lin L 2004 Post-packaging frequency tuning of microresonators by pulsed laser deposition *J. Micromech. Microeng.* **14** 1742–7
- [224] Ho G K, Perng J K and Ayazi F 2010 Micromechanical IBARs: modeling and process compensation *J. Microelectromech. Syst.* **19** 516–25
- [225] Liu R, Paden B and Turner K 2001 MEMS resonators that are robust to process-induced feature width variations *Proc. 2001 IEEE Int. Frequency Control Symp. and PDA Exhibition* pp 556–63
- [226] Ho G K, Perng J K C and Ayazi F 2007 Process compensated micromechanical resonators *Proc. MEMS 2007 (21–25 January 2007)* pp 183–6
- [227] Quevy E P and Howe R T 2005 Redundant MEMS resonators for precise reference oscillators *IEEE Radio Frequency Integrated Circuits Symp.* pp 113–6